Anomalous transit-time dispersion in amorphous solids

Harvey Scher
Xerox Webster Research Center, 800 Phillips Road, Webster, New York 14580

Elliott W. Montroll
Institute for Fundamental Studies, Department of Physics and Astronomy, University of Rochester, Rochester, New York 14627*

(Received 13 January 1975)

Measurements of the transient photocurrent $I(t)$ in an increasing number of inorganic and organic amorphous materials display anomalous transport properties. The long tail of $I(t)$ indicates a dispersion of carrier transit times. However, the shape invariance of $I(t)$ to electric field and sample thickness (designated as universality for the classes of materials here considered) is incompatible with traditional concepts of statistical spreading, i.e., a Gaussian carrier packet. We have developed a stochastic transport model for $I(t)$ which describes the dynamics of a carrier packet executing a time-dependent random walk in the presence of a field-dependent spatial bias and an absorbing barrier at the sample surface. The time dependence of the random walk is governed by hopping time distribution $\psi(t)$. A packet, generated with a $\psi(t)$ characteristic of hopping in a disordered system [e.g., $\psi(t) \sim t^{-(1+\alpha)}$, $0 < \alpha < 1$], is shown to propagate with a number of anomalous non-Gaussian properties. The calculated $I(t)$ associated with this packet not only obeys the property of universality but can account quantitatively for a large variety of experiments. The new method of data analysis advanced by the theory allows one to directly extract the transit time even for a featureless current trace. In particular, we shall analyze both an inorganic (a-As_2Se_3) and an organic (trinitrofluorenone-polyvinylcarbazole) system. Our function $\psi(t)$ is related to a first-principles calculation. It is to be emphasized that these $\psi(t)$'s characterize a realization of a non-Markoffian transport process. Moreover, the theory shows the limitations of the concept of a mobility in this dispersive type of transport.

I. INTRODUCTION

The development of modern photocopying machines has motivated experimental work on amorphous materials, some of which display anomalous transport properties. In such a machine the surface of a film of amorphous material is charged by a corona and excited by a light pulse which creates pairs of charge carriers as exhibited in Fig. 1(a). The electric field due to the deposited charge transports one of the carrier components, say the positive charge, away from the optically excited surface, leaving the negative charge behind. A powder of negatively charged particles (toner) is then attached to the remaining positive spots (the latent image) on the film. The toner is finally fixed on a paper which passes over the charged surface. It is natural that in the investigation of amorphous materials used in such a technology, one should have measured the mobility of the positive carrier (holes) in films of the materials. From these measurements, experimenters were surprised to find that carrier mobilities in some of these amorphous materials depend on the thickness of the material instead of being an intrinsic property of the material. It is this observation, as well as others, which we describe as "anomalous transport properties."

Two of the materials used commercially are As_2Se_3, and an organic charge-transfer complex of trinitrofluorenone and polyvinylcarbazole (TNF-PVK).

Measurements of the transient current in insulators, due to injected charge, have often been the only means to probe the transport properties of these materials. Earlier investigations of sulfur[1] and amorphous selenium (a-Se)[2] have yielded detailed information on the drift mobility of both electrons and holes and on deep-trapping lifetimes. Charge injection with strongly absorbed light has, in addition, enabled one to separate the transport of charge from the photogenerated supply efficiency.[3] Recent drift-mobility observations in[4] a-Si have provided the only substantial experimental evidence for the often-discussed "mobility edge" in amorphous semiconductors.[5]

Let us now proceed to summarize the experimental background to our theory and the *main ideas* of our theoretical model. This model will be analyzed in detail in Secs. II and III.

A. Experiments

The basic measurement technique is illustrated in Fig. 1(b). The sample is sandwiched between two planar contacts, one or both of which are semitransparent. A short, strongly absorbed, light flash causes a conduction current to flow in the sample, which is held at a constant voltage V if the circuit RC time is much less than the time scale of the experiment. The measured current $I(t)$, under these conditions, is simply the space-averaged conduction current

$$I(t) = \frac{1}{L}\int_0^L j_c(x,t)\,dx\,, \tag{1}$$

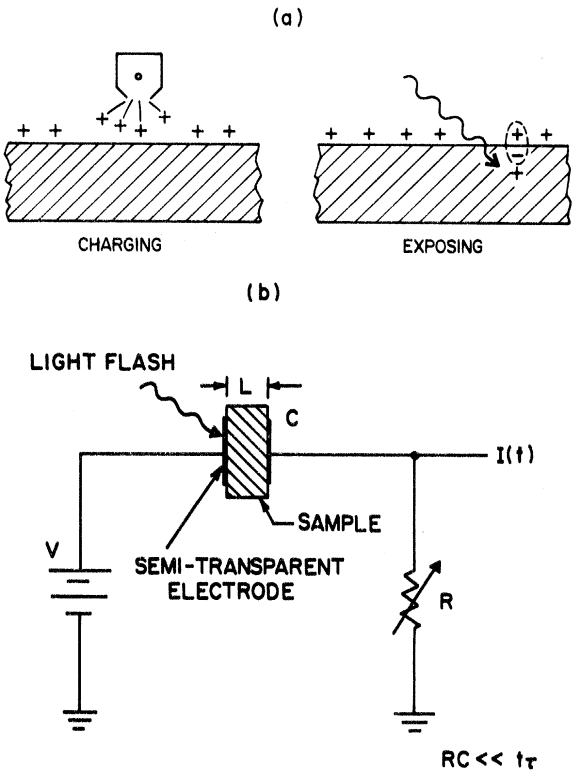

FIG. 1. (a) Initial steps in the xerographic copying process: (1) A high-resistivity photoconductor is charged by a corotron. (2) An absorbed photon creates an electron-hole pair. The electron neutralizes the positive ion on the surface while the hole moves through the photoconductor to neutralize the countercharge on the electrode. The remaining positive ions constitute the latent image. (b) Schematic diagram for a transient photoconductivity measurement. A light flash of duration much shorter than the transit time t_τ is absorbed in a depth much less than the sample thickness L. Carriers of one sign move across the sample, inducing a time-dependent current $I(t)$ in the external circuit.

where L is the sample thickness. An idealized $I(t)$ following the light flash is shown in Fig. 2. It depicts a sheet of charge moving with constant velocity and departing from the sample at the transit time t_τ. An unambiguous drift mobility μ can be determined by the relation

$$\mu = L^2/t_\tau V . \tag{2}$$

Departures from the idealized current shape in Fig. 2 might be the result of several influences: (a) RC response time, (b) loss of carriers due to deep trapping, (c) variation in drift mobility as a function of x due to sample inhomogeneity, (d) local electric-field variation due to trapped space charge, and (e) spreading of the sheet of charge to a width comparable to L. (We shall restrict ourselves to the "small-signal" case, i.e., we will not consider spreading due to the mutual Coulomb repulsion of the trap-free-space-charge-limited or "large signal" case.[6])

The first two of the above influences usually determine the practical limitations of the transient experiment. One must have

$$RC \ll t_\tau \ll \tau_D , \tag{3}$$

where τ_D is the deep-trapping lifetime. The next two influences can cause a variation in the current level. The carriers can still move across the sample as a sheet of charge. However, the changes in drift velocity as a function of x will cause a variation in the step height of the current in Fig. 2 but not necessarily change the sharp drop at the transit time. Recently, Pai[7] has used small incremental steps in the current to map a profile of charged impurities in a-Se.

The influences so far discussed are characterized by definite mechanisms. The last item, which involves a discernible spreading of the sheet of charge, is really a generic symptom of a number of possible causes rather than any one specific departure from the ideal behavior shown in Fig. 2. The spreading can arise from statistical fluctuations associated with a variety of processes, including multiple trapping, hopping, or dispersion due to material inhomogeneity (e.g., granular effects, nonuniform thickness). This type of spreading can result in a decreasing current level and a considerable smearing of the "transit edge."

In recent experiments on an increasingly wider class of amorphous materials, As_2Se_3,[8,9] PVK,[10] and TNF-PVK,[11] one typically obtains the current trace shown in Fig. 3 instead of the current shape shown in Fig. 2, which is realized in S and in a-Se at room temperature. The exhibited trace is derived from measurements[18] on As_2Se_3; however, except for scaling factors, it is identical in appearance to those obtained in PVK,[10] TNF-PVK.[11] Examining the features of Fig. 3, we observe that the current spike, immediately after the onset of the short light pulse, is followed by a soft "plateau" in

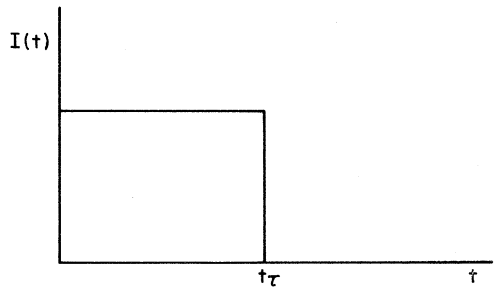

FIG. 2. Idealized transient-current trace measured with the technique shown in Fig. 1(b). The trace depicts a sheet of charge moving with constant velocity until it leaves the sample at time t_τ.

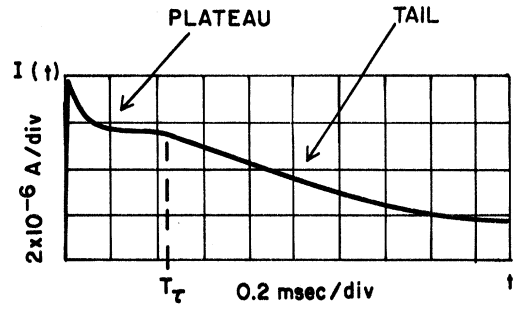

FIG. 3. Highly dispersive transient photocurrent trace $I(t)$ measured on As_2Se_3 by Scharfe.

the current level, then a "shoulder" or transition region, and finally a ubiquitous long "tail." These distortions of the idealized response, indicated in Fig. 2, immediately suggest some statistical process causing a spread in the transit times (or a distribution in surface release times[12]) as discussed above. The tail represents the dribble of the "slow" carriers. The shoulder region or onset of the tail has been chosen as the transit time; however, as will be shown, one often does not even see a shoulder.

A very revealing treatment of the $I(t)$ data advanced by Scharfe[8] is shown by the plot in Fig. 4. The current is normalized to $I(t)_\tau$ and the time is measured in relative units of t_τ. Scharfe has chosen t_τ to be the time of the onset of the tail. The $I(t)$ data, corresponding to a wide range of transit time (obtained by changing E or L), is shown in Fig. 4 to collapse into one curve in this type of plot. We designate this feature as "universality." This universality is the clue, as shown below, that an unusual statistical process is taking place, a process in which the ratio of the mean position $\langle l \rangle$ of the propagating packet of carriers to the rms spread σ is independent of time, i.e.,

$$\langle l \rangle / \sigma = \text{const} \tag{4}$$

for t of the order of t_τ, i.e., $t = O(t_\tau)$.

B. Theory

The universality is most clearly exhibited on a log$I$-log$t$ plot. The nature of the carrier transport is also easier to interpret on these plots. In Fig. 5, we have a plot of this kind for an inorganic film and in Fig. 6, for an organic. A schematic form of these current curves is displayed in Fig. 7.

These curves will be analyzed in the main body of this paper through a hopping-time distribution function $\psi(t)$. In an amorphous material there is a dispersion in the separation distances between nearest-neighbor localized sites available for hopping carriers and a dispersion in the potential barriers between these sites. Both of these variables strongly affect the hopping time, the time between a carrier arrival on successive sites. Hence, the distribution of these hopping times, $\psi(t)$, would have a long tail. We will propose tails of the form

$$\psi(t) \sim \text{const} \times t^{-(1+\alpha)}, \quad 0 < \alpha < 1 \tag{5}$$

indicating an extremely large hopping-time dispersion. Classical Gaussian propagation as exhibited in Fig. 8 is associated with an asymptotic exponential tail with $\psi(t) \sim e^{-\lambda t}$. The $\psi(t)$ in Eq. (5) will be related to a first-principles calculation of the distribution function in a disordered system in Sec. III. The main point to emphasize here is the contrast between Eq. (5) and a $\psi(t) \sim e^{-\lambda t}$, which is characteristic of a system with a single transition rate λ.

When the inverse-power tail (5) exists, a considerable fraction of the carriers remain at the point of their formation for a long time. Those carriers whose local environment at their initial point permits their immediate motion (fast hops) will sooner

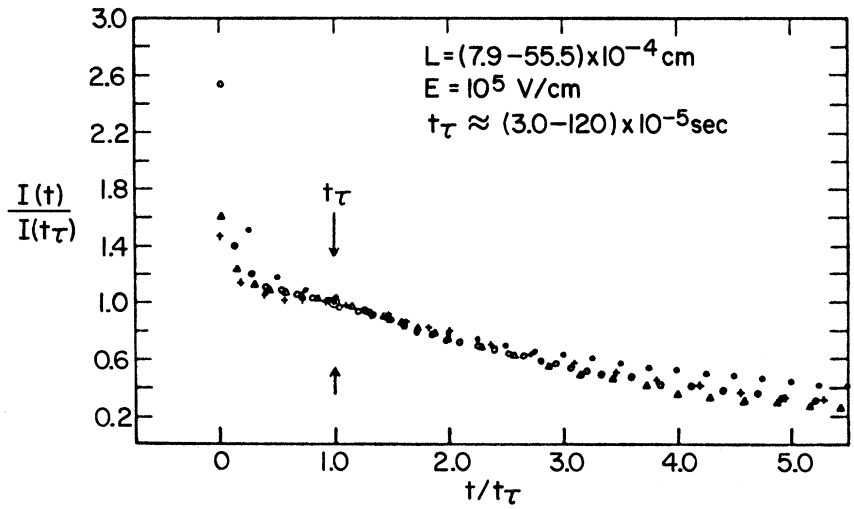

FIG. 4. Superposition of normalized current traces, for a range of transit time t_τ, as a function of t/t_τ. The invariance of the shape of $I(t)$ to t_τ is designated as universality. E is the electric field and L is the sample thickness.

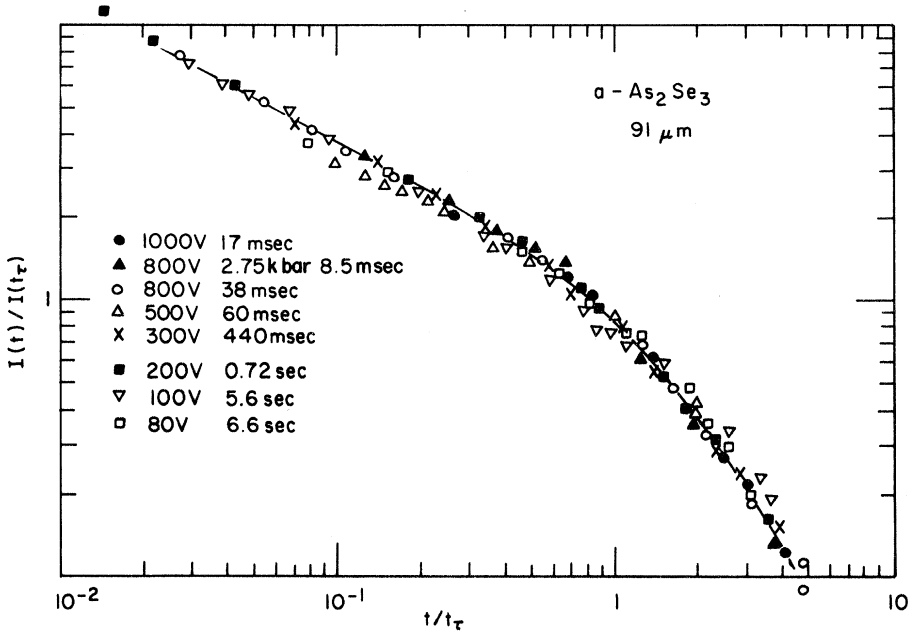

FIG. 5. A log$I$-log$t$ plot for a-As_2Se_3 for the range of transit time listed in the figure. The measurements by Pfister also include a data set at high pressure (2.75 kbar). The solid line is the theoretical curve.

or later find themselves immobilized at some site (long hops), thus reducing their contribution to the current, until they escape. The propagating packet associated with Eq. (5) has the form exhibited in Fig. 9. While the peak of the Gaussian packet of Fig. 8 and the mean carrier of the packet are located at the same position and move with the same velocity, the mean carrier of the packet of Fig. 9 propagates with a velocity which decreases with time as it separates from the peak which remains nearly fixed at the point of origin of the carriers.

The type of current trace expected for a moving Gaussian packet is shown in Fig. 10. As the mean moves with constant velocity, the current is constant until the mean carrier encounters the absorbing barrier at the sample surface; then, the current level drops to zero. The rounding of the "transit edge" reflects the spread in the transit times of the carriers in the packet. As observed in Fig. 8, for a Gaussian packet, the ratio $\sigma/\langle l\rangle$ decreases with time ($\sigma/\langle l\rangle \sim t^{-1/2}$). Hence, in the plot of $I(t)/I(t_\tau)$ vs t/t_τ shown in Fig. 10, there will be a relative sharpening of the transit edge for the longer transit times as indicated by curve (1), while the current trace for shorter t_τ [curve (2)] will show more relative dispersion. *Universality of the current is incompatible with a propagating Gaussian packet!* In Fig. 9, the packets spread in the same manner as the moving mean; $\sigma/\langle l\rangle$ is independent of time, and the current traces associated with these packets are universal.

In an infinite sample, the decrease in velocity of the mean carrier in these packets (Fig. 9) implies a continuous reduction of the current. It will be shown in Sec. II that the current variation derivable from Eq. (5) is

$$I(t) \sim \text{const} \times t^{-(1-\alpha)} . \tag{6}$$

This is the form plotted in Fig. 7 when t/t_τ is less than 1.0. In a sample of finite thickness, an additional reduction of current results from the loss of carriers into the absorbing barrier when a group of the fastest carriers reaches the barrier. The time t_τ is to be identified with this change in the time dependence of $I(t)$. For $t \gg t_\tau$ we will show

$$I(t) \sim \text{const} \times t^{-(1+\alpha)} . \tag{7}$$

Note that a check of the model would be the observation that, in a plot of log$I$ as a function of log$t$, the sum of the slopes at times $t/t_\tau < 1$ and at times $t/t_\tau \gg 1$ would be $-[(1+\alpha)+(1-\alpha)] = -2$. The data

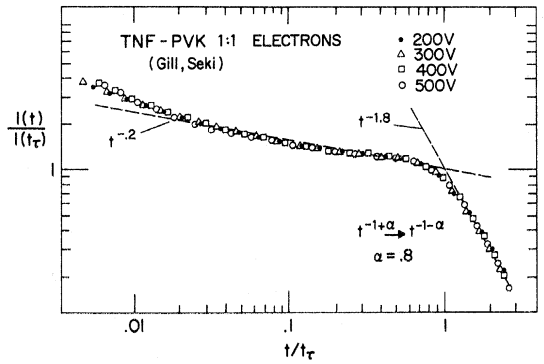

FIG. 6. A log$I$-log$t$ plot for 1:1 TNF-PVK measured by Gill and taken from a paper by Seki. The slopes of the dashed lines are -0.2, and -1.8, respectively.

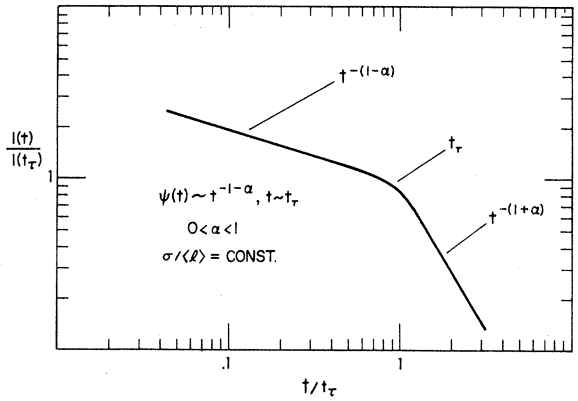

FIG. 7. A log$I$-log$t$ plot indicating the current $I(t)$ associated with a packet of carriers moving, in an electric field, with a hopping-time distribution function $\psi(t) \sim t^{-1-\alpha}$, $0<\alpha<1$, towards an absorbing barrier at the sample surface.

obtained for a number of As_2Se_3 samples exhibited in Fig. 5 indicate that $\alpha = 0.45$, while Fig. 6 shows that for amorphous TNF-PVK, $\alpha \simeq 0.80$.

Traditional transport theory, which is characterized by the motion of Gaussian packets, is generally described through a Markoffian transport master equation which might be written as

$$d\tilde{P}(l, t)/dt = \lambda \sum_{l'} [\, p(l-l')\, \tilde{P}(l', t) - p(l'-l)\, \tilde{P}(l, t)\,] . \tag{8}$$

Here l represents a cell number in a system which is broken into equal-sized cells, and $\tilde{P}(l, t)$ is the

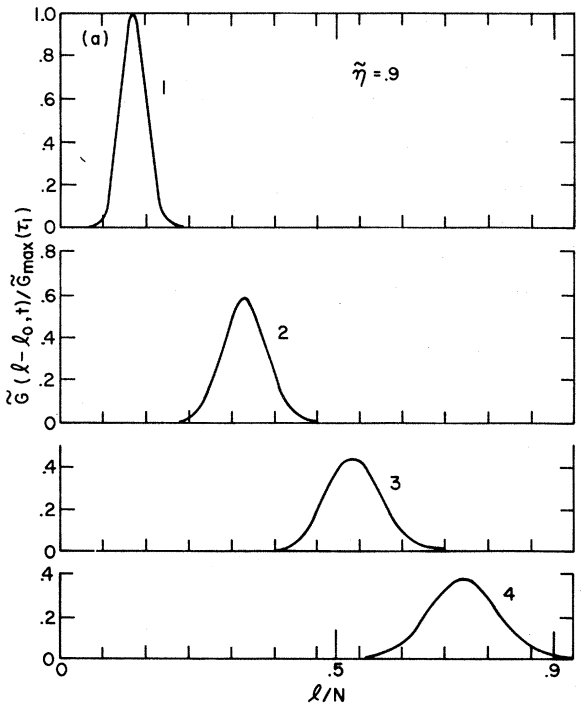

FIG. 8. Propagator for a carrier packet $\tilde{G}(l-l_0, t)$ vs l/N for a range of time $t/t_\tau = (2n-1)/10$, $n = 1, 2, 3, 4$. The "transit time" is defined by $\langle l(t_\tau)\rangle/N = 1$. The random walk is based on $\psi(t)/\lambda = e^{-\lambda t}$. The plot is scaled by the peak value of $\tilde{G}(l-l_0, t)$ at the earliest time. The spatial bias factor $\tilde{\eta} = 0.9$.

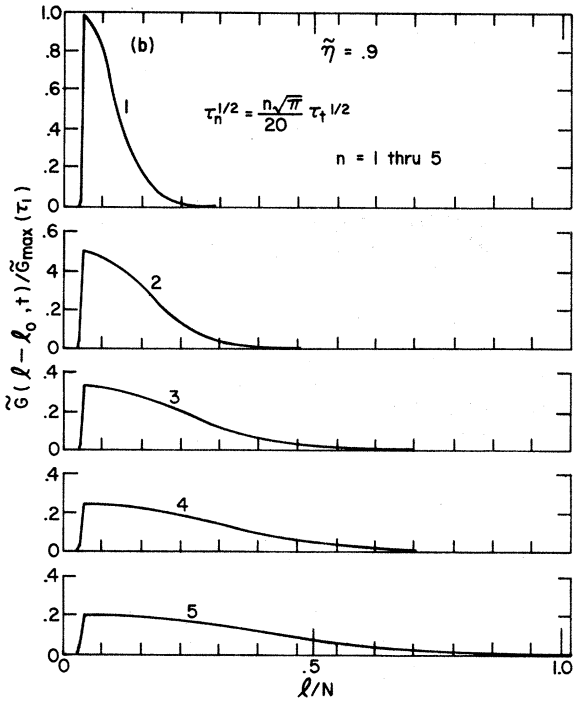

FIG. 9. Propagator for a carrier packet $\tilde{G}(l-l_0, t)$ vs l/N for a range of time $\tau_n^{1/2} = (n\sqrt{\pi}/20)\,\tau_t^{1/2}$ $n = 1$–5, and τ_t defined in the text. The random walk is based on $\psi_2(t) \sim \pi^{-1/2} t^{-3/2}$. The plot is scaled by the peak value of $\tilde{G}(l-l_0, t)$ at the earliest time. The spatial bias factor $\tilde{\eta} = 0.9$.

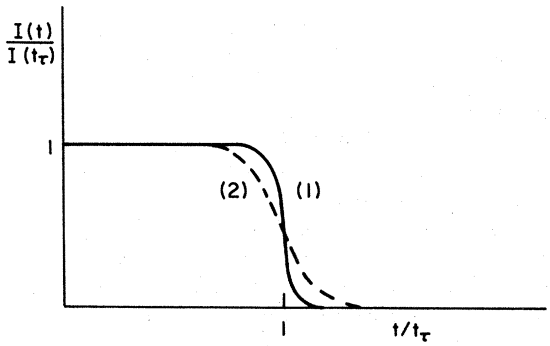

FIG. 10. Normalized current trace $I(t)/I(t_\tau)$ vs t/t_τ expected for a propagating Gaussian packet. Curve (1) corresponds to the longer t_τ and curve (2) corresponds to the shorter t_τ. This figure illustrates the incompatibility of a Gaussian with the universality of $I(t)$.

probability that a cell l is occupied by a carrier at time t. The first term on the right-hand side represents the flow rate into cell l from transitions from l', while the second represents flow out of l into l'; λ is a proportionality constant. The general non-Gaussian, non-Markoffian transport process which we proposed above can be described by a generalized master equation[13] with a relaxation function $\phi(t)$:

$$d\tilde{P}(l,t)/dt = \int_0^t \phi(t-x) \sum_{l'} [\, p(l-l')\, \tilde{P}(l',x) - p(l'-l)\, P(l,x)]\, dx \,. \tag{9}$$

The relaxation function $\phi(t)$ and the hopping-distribution functions are related through their Laplace transforms $\phi^*(u)$ and $\psi^*(u)$ with

$$\phi^*(u) = u\psi^*(u)/[1-\psi^*(u)] \,. \tag{10}$$

An exponential $\psi(t) = \lambda e^{-\lambda t}$ yields $\phi(t) = 2\lambda\delta(t)$, so that Eq. (9) reduces to Eq. (8) in that case.

It is now apparent that one must go beyond the traditional transport concepts embodied in Eq. (8), in order to generate propagating carrier packets that can account for all the experimental evidence.

In Sec. II we will define the model, present the mathematical problem generated by the application of the model, and review the essential features of the analytic solution of the problem. In Sec. III we will exhibit the main theoretical results of our model, discuss in some detail their conceptual implications, and we will compare these results with the available experimental data on a wide class of amorphous insulators. The very satisfactory agreement with theory (as already shown in Figs. 4–7) will be advanced as strong evidence that the same phenomenon is indeed occurring in each of the different materials. We will further indicate the direction of future work on this unusual phenomenon.

II. MODEL

An amorphous insulating material might be considered a network of localized sites for electrons or holes. Electron or hole transport in such a material could be characterized by a succession of hops from one site to another. The distances between various neighboring sites have some variation about a mean value, and the effective intersite transition rates, which sensitively depend on these distances, will suffer a wide statistical dispersion. This in turn yields a broad distribution of hopping times.

In our model we postulate our material to be divided into a regular lattice of equivalent cells, with each cell containing many randomly distributed localized sites available for hopping carriers.

Carrier transport is a succession of carrier hops from one localized site to another and finally from one cell to another. We define the hopping time to be the time interval between the moment of arrival of a carrier into one cell and the moment of arrival into the next cell into which it lands. The random distribution of sites and hence the disorder of an amorphous material is incorporated into a hopping-time *distribution function* $\psi(t)$. Then $\psi(t)\,dt$ is the probability that after a carrier arrives in a given cell, it will arrive in its next cell in the time interval $(t, t+dt)$. We identify the cells by dimensionless lattice vectors with components l_1, l_2, l_3, where $l_i = 1, 2, \ldots, N_i$. The set $\{N_i\}$ defines the size of the lattice in units of the individual cell dimensions. At first, when we consider our lattice to be periodic, the numbers N_1, N_2, and N_3 will represent the number of cells in various directions.

In the practical computation of $\psi(t)$, as in Ref. 14, one could have a single site per cell. In that case, $\psi(t)$ is the distribution of intersite hopping times. One can consider hopping on a lattice because the main effects of intersite spatial variations are to produce enormous variations in the hopping times. These effects are incorporated into a calculation of $\psi(t)$ for a random medium as discussed in Ref. 14 and in Sec. III.

Transient photoconductivity, according to this general transport model, would be characterized by a group of carriers (Fig. 11) executing a three-dimensional time-dependent random walk biased by an electric field E. The directional bias will be characterized by a dimensionless asymmetry factor $\tilde{\eta}(E)$. A group of carriers is pictured in Fig. 11 to be initially near the (+) electrode of a planar capacitor. They drift a distance L to the right along the x axis toward the (−) electrode, where they become absorbed.

The analytic description of an asymmetric non-Markoffian continuous-time random walk in the presence of planar absorbing barriers has been given by the authors (Ref. 15). We now review the main features of this process.

The basic quantity of our theory is $\tilde{G}(l,t)$, the probability that a walker is found at l at time t if at time $t=0$ it was at the origin. The function $\tilde{G}(l,t)$ completely specifies the propagation of the carrier packet (in the absence of the absorbing boundary). This quantity is related to two functions, $\psi^*(u)$ and $G(l,z)$, through the inverse-Laplace-transform contour integral[15]

$$\tilde{G}(l,t) = \frac{1}{2\pi i} \int_{c-i\infty}^{c+i\infty} (du/u)\, e^{ut}\, [1-\psi^*(u)]\, G(l, \psi^*(u)) \,. \tag{11}$$

The function $\psi^*(u)$ is the Laplace transform of the hopping-time distribution $\psi(t)$,

$$\psi^*(u) = \int_0^\infty e^{-ut}\, \psi(t)\, dt \,, \tag{12}$$

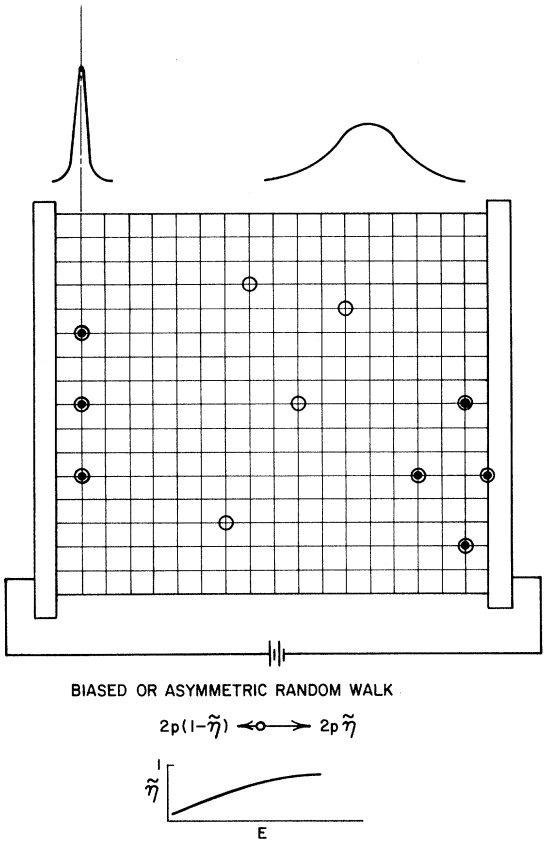

FIG. 11. Schematic diagram for the random-walk model of transient photoconductivity. The diagram is a composite in time. The carriers (●) are injected as a narrow distribution at $t=0$ in the localized sites (○). The packet spreads and propagates to the right, $t>0$, with a spatial bias $\tilde{\eta}$, towards an absorbing barrier.

and $G(l, z)$ is a random-walk generating function, which for periodic boundary conditions has the form

$$G(l, z)=\frac{1}{N_1N_2N_3}\sum_{s_1=1}^{N_1}\sum_{s_2=1}^{N_2}\sum_{s_3=1}^{N_3}\frac{e^{i\vec{l}\cdot\vec{k}}}{1-z\lambda(k)}, \tag{13}$$

with $k_j=2\pi s_j/N_j$. The structure function $\lambda(k)$ is the Fourier representation of the transition probability of hops from cell to cell:

$$\lambda(k)=\sum_l p(l)\,e^{i\vec{l}\cdot\vec{k}}\,. \tag{14}$$

Here $p(l)$ is the probability of a hop from a given cell to one displaced by a vector l from it, with

$$\sum p(l)=1\,. \tag{15}$$

Our hopping process is then characterized by the two functions $\psi(t)$ and $p(l)$, $\psi(t)$ being the hopping-time distribution at any cell and $p(l)$ being the transition probability of a hop by a vector distance l. All cells are defined to be equivalent, so that $\psi(t)$ and $p(l)$ are universal functions for all cells. All the disorder is included in the fact that the functions are *distributions*, and these distributions are determined from an ensemble of random systems (cf. Sec. III).

The carrier current $I(t)$ in the x direction (l_1) in an assembly of hopping charges is proportional to the time rate of change of the mean of the carrier packet

$$I(t)\propto d\langle l_1\rangle/dt\,, \tag{16}$$

where

$$\langle l_1\rangle=\sum_{l_1=1}^{N_1}\sum_{l_2=1}^{N_2}\sum_{l_3=1}^{N_3} l_1\,\tilde{G}(l, t)\,. \tag{17}$$

The field is in the x direction; hence $\langle l\rangle=\langle l_1\rangle$.

We shall now compute Eqs. (11) and (16) for a set of prototype forms of $\psi(t)$, illustrating the dramatic change in the carrier-packet propagation with characteristically different $\psi(t)$. Throughout our discussion we assume that carrier displacements are between nearest-neighbor cells with probabilities (with $\tilde{\eta}>\frac{1}{2}$)

$$p(0, \pm 1, 0)=p(0, 0, \pm 1)=q\,, \tag{18}$$

$$p(1, 0, 0)=2\tilde{\eta}p,\ p(-1, 0, 0)=2(1-\tilde{\eta})p \tag{19}$$

[all other $p(l_1, l_2, l_3)$ vanishing]. These transition probabilities correspond to nearest-neighbor hopping on a simple cubic lattice with a bias for hops in the $+x$ direction over that in the $-x$ direction, due to the electric field, i.e., $\tilde{\eta}\equiv\tilde{\eta}(E)$. The adoption of Eqs. (18) and (19) is consistent with the assertion that the spatial fluctuations are trivial compared to the hopping-time fluctuations.[14] The asymmetry which is introduced by E in the basic hopping-transition probabilities of the system is reflected in the phenomenological function $\tilde{\eta}(E)$. Discussion and generalization of this approach is included at the end of the next section.

The two types of $\psi(t)$ we shall consider are

$$\psi_1(t)=We^{-\tau} \tag{20}$$

and

$$\psi_2(t)=4W_M\,e^{\tau}i^2\,\mathrm{erfc}\,(\tau^{1/2})\,, \tag{21}$$

where W and W_M are rate constants, τ is a dimensionless time (Wt or W_Mt), and $i^2\mathrm{erfc}z$ is the second repeated integral of the complementary error function, the nth repeated integral being

$$i^n\,\mathrm{erfc}z\equiv(2/\pi^{1/2}n!)\int_z^\infty(t-z)^ne^{-t^2}dt\,. \tag{22}$$

The distribution $\psi_1(t)$ is a rapidly decaying function of τ. It generates a random walk with only *one* intersite-hopping transition rate, W. It decays rapidly because in such a process the probability of hopping is in sharp contrast for the two time regimes, $t<W^{-1}$ or $t>W^{-1}$. The choice $\psi_1(t)$ implies

that

$$\langle l\rangle = \bar{l}\tau\,, \tag{23a}$$

where

$$\bar{l} = 2p(2\tilde{\eta} - 1)\,, \tag{23b}$$

$\bar{l}$ being the mean displacement for a single hop and computed with the model characterized by Eqs. (18) and (19); hence,

$$d\langle l\rangle/dt = \bar{l}W\,. \tag{23c}$$

The dispersion is

$$\sigma^2 = \langle (l_1 - \langle l\rangle)^2\rangle = 4p\tau\,, \tag{24}$$

and

$$\sigma/\langle l\rangle \sim \tau^{-1/2}\,. \tag{25}$$

In Fig. 8 we have plotted $\tilde{G}(l, t)$ for this case. As can be judged from the figure, the curves become Gaussian after a δ-function pulse initially near the origin has propagated a small fraction of N. Note that in Eq. (23c) the propagation rate is constant at all time. Also note that for a Gaussian, $\sigma/\langle l\rangle$ decreases with increasing τ. The results summarized above are valid not only for an exponential $\psi(t)$, but remain appropriate for $\psi(t)$ generally when at least the first two moments of $\psi(t)$ exist, and $t > \bar{t}$, defined by

$$\bar{t} = \int_0^\infty t\psi(t)\,dt\,. \tag{26}$$

All moments of the exponential distribution $\psi_1(t)$ exist.

When $\psi(t)$ has a long tail [e.g., $\psi(t) \sim t^{-\beta}$, $\beta \leqq 3$, as $t \to \infty$], the above results are no longer applicable. The function $\psi_2(t)$, defined by Eq. (21), is of this type with the asymptotic tail

$$\psi_2(t)/W_M \sim \pi^{-1/2}\tau^{-3/2}\,, \quad \tau \gg 1\,, \tag{27}$$

and has been investigated in considerable detail by the authors.[15] We will show later that experimental results always correspond to $\tau \gg 1$. The fact that $\psi_2(t)$ has no finite positive integral moments, not even the first, leads to the unusual character of the propagated pulse exhibited in Fig. 9. The mean position of the propagating packet is, if $\tau \gg 1$,

$$\langle l\rangle \sim \bar{l}(\tau/\pi)^{1/2}\,. \tag{28a}$$

The peak in the distribution, however, remains near the initial position. Hence the current $I(t)$, which is proportional to

$$d\langle l\rangle/dt \sim \tfrac{1}{2}\bar{l}(\pi\tau)^{-1/2}\,, \tag{28b}$$

decreases with increasing time until it finally vanishes, even in the absence of an absorbing boundary!

This observation that the mean position of a carrier in the packet is a fractional power of time will be the basis of our discussion of anomalously propagating packets. The behavior of Eq. (28a) is a consequence of the long tail of $\psi_2(t)$ as exhibited in Eq. (27). The slowly varying time dependence of $\psi_2(t)$ corresponds to a large dispersion in hopping times. One can physically understand the decaying current in Eq. (28b) on this basis. At early times in the transport process, most carriers are moving with the relatively more probable short hopping times. However, with increasing t all carriers eventually encounter at least one long hopping time. Since long hopping times are analogous to a deep trap, the carrier is immobilized temporarily. Hence, as $t \to \infty$, most carriers become so immobilized that the current becomes very small.

Figure 9 shows that the peak in the packet remains near its starting position while the mean advances according to Eq. (28a). Thus, the dispersion grows in the same manner as the mean carrier displacement, $\langle l\rangle$, so that

$$\sigma^2 \sim \bar{l}^2\tau(\tfrac{1}{2}\pi - 1)/\pi\,. \tag{29}$$

Hence

$$\sigma/\langle l\rangle \sim (\tfrac{1}{2}\pi - 1)^{1/2}\,, \tag{30}$$

a constant independent of t. This is to be compared with the classical Gaussian result Eq. (25). Equation (30) is the basis for our understanding of the universality of $I(t)$ provided in Eq. (4). It is now clear that a distribution of the type $\psi_2(t)$ can generate carrier packets displaying the appropriate qualitative transport behavior.

An immediate mathematical generalization of $\psi_2(t)$ is the class of hopping-time distribution functions with long tails which decay asymptotically as $t \to \infty$ in the following manner:

$$\psi(t) \sim [At^{1+\alpha}\Gamma(1-\alpha)]^{-1}, \quad 0 < \alpha < 1. \tag{31}$$

A detailed physical justification for the application of members of this class to our anomalous transport phenomenon is given in the beginning of the next section. Now we might ask if results such as Eqs. (28) and (30) are a consequence of the general behavior of Eq. (31). Shlesinger[16] has shown by applying certain Tauberian theorems in a manner presented in Appendix A of this paper, that Eq. (31) implies that

$$\langle l\rangle \sim \bar{l}At^{\alpha}/\Gamma(\alpha+1) \tag{32}$$

and

$$\frac{\sigma}{\langle l\rangle} \sim \{[2\Gamma^2(1+\alpha)/\Gamma(1+2\alpha)] - 1\}^{1/2}\,, \tag{33}$$

with $\bar{l} \neq 0$. A $\psi(t)$ of the form (31) thus yields a fractional-power time dependence of $\langle l\rangle$ and a ratio of dispersion to mean independent of time (33).

We now complete the mathematical development of our model by calculating the important influence of the absorbing plane at $l_1 = N \equiv 0$ (N being the number of cells in the x direction). When $\langle l \rangle \sim N$, one switches from the small-slope portion of $I(t)$ (Fig. 7) to the large-slope portion, since carriers disappear in large numbers into the boundary after that time. We have shown[15] that for an injected carrier initially at the plane $l_1 = l_0$, that the free-space propagator $\tilde{G}(l - l_0, t)$ is to be replaced by

$$\tilde{P}(l, t) = \tilde{G}(l - l_0, t) - \int_0^t \tilde{G}(l, t - x)\tilde{F}(N - l_0, x)\, dx, \tag{34}$$

where $\tilde{F}(l, t)$ is the first passage-time distribution function for the transition $l_0 \to N$ ($N \equiv 0$). The probability $\tilde{P}(l, t)$ for a carrier, starting at l_0 at $t = 0$, to be found at l at time t, is equal to the unperturbed propagator for the transition $l_0 \to l$ minus the contribution of all paths that have crossed the boundary at N. These are represented by the integral in Eq. (34). All the paths that cross the boundary can be specified by first grouping them into a probability per unit time of a carrier reaching N from l_0 for the first time, $\tilde{F}(N - l_0, x)$,

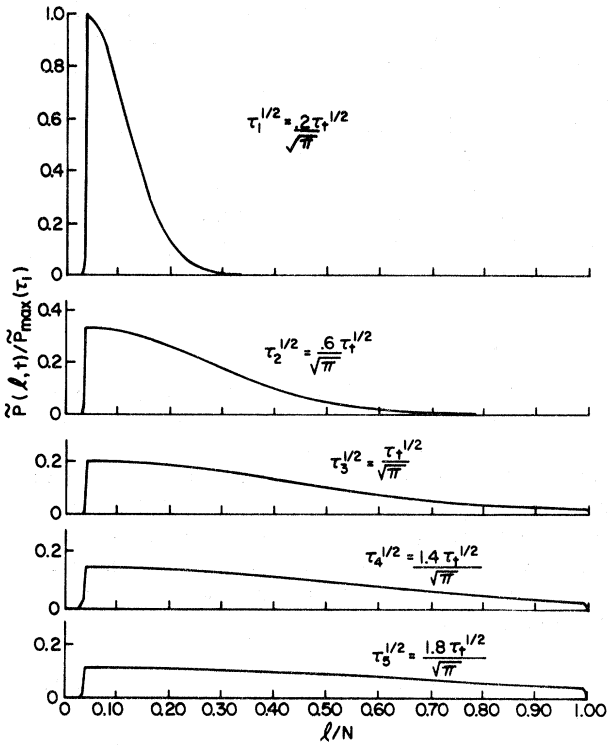

FIG. 12. Propagator for a carrier packet $\tilde{P}(l, t)$ in the presence of absorbing barriers at $l/N = 0, 1$, for a range of time $\tau_n^{1/2} = 0.2(2n-1)\tau_t^{1/2}/\sqrt{\pi}$, $n = 1, 5$. The transit time τ_t is defined in the text. The random walk is based on $\psi_2(t) \sim \pi^{1/2}\,\tau^{-3/2}$. The spatial bias factor $\tilde{\eta} = 0.9$.

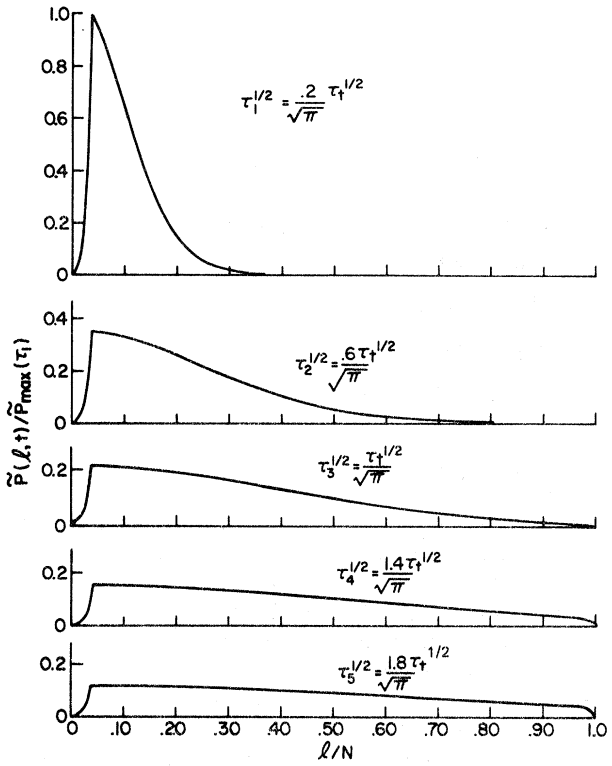

FIG. 13. Same as Fig. 12 with $\tilde{\eta} = 0.6$.

at some earlier time x, and then returning to l in the remaining time $(t - x)$ without concern for whether or not it had again encountered the boundary. Note that $\tilde{G}[-(N - l), t - x] \equiv \tilde{G}(l, t - x)$. The integration in Eq. (34) represents a sum over all times $x < t$ when the first crossing might have been made.

The method we use to compute $\tilde{P}(l, t)$ is the same as the one used to construct the graphs of $\tilde{G}(l, t)$ shown in Figs. 8 and 9. The first step is to construct the spatial Fourier transform (FT) of $\tilde{P}(l, t)$,

$$\Gamma(k, \tau) = \sum_{l=1}^{N} e^{-ikl}\,\tilde{P}(l, t), \tag{35}$$

analytically from a chosen $\psi(t)$. Then this FT is inverted numerically. This procedure is applied in Appendix B for the interesting function $\psi_2(t)$ to obtain the formula (B19). In Figs. 12–14 we plot the time series of $\tilde{P}(l, t)$ for various values of the asymmetry factor $\tilde{\eta}$. Note that the shape of the propagating packet differs from the free-carrier form (in Fig. 9) of $\tilde{G}(l, t)$ only in the truncation region in which the packet overlaps the absorbing boundaries at the ends of the sample. We are primarily interested in the effect of the boundary on $\langle l \rangle$ and, thus, on $I(t)$. For $\psi_2(t)$ we can compute $\langle l \rangle$ analytically from

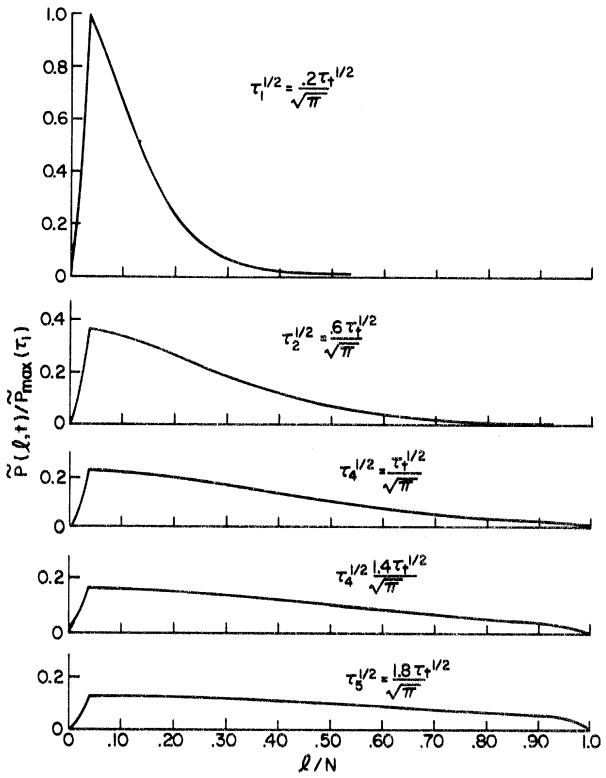

FIG. 14. Same as Fig. 12 with $\tilde{\eta} = 0.53$

$$\langle l \rangle = \left. \frac{\partial \Gamma(k,\tau)}{\partial k} \right|_{k=0} , \tag{36}$$

using Eq. (B19) of Appendix B. An alternative calculation of $\langle l \rangle$ can also be made directly from Eq. (34) by inserting the asymptotic value of the mean computed with $\tilde{G}(l,t)$ in Eq. (28a) and the asymptotic value of $\tilde{F}(N-l_0,t)$, both valid for $\tau \gg 1$, into that formula. When $\tau \gg 1$, the hopping-time distribution $\psi_2(t)$ is known [Eqs. (B5)–(B9), cf. also Ref. 15] to yield the asymptotic formula

$$\tilde{F}(N-l_0,\tau)/W_M \sim (\beta/\pi^{1/2}\tau^{3/2})\, e^{-\beta^2/\tau} , \quad \tau \gg 1, \tag{37}$$

where $\beta \equiv (N-l_0)/\bar{l}$. The expression (37) is vanishingly small until

$$[(N-l_0)/\bar{l}]^2/\tau \sim 1 \tag{38}$$

or, from Eq. (28a)

$$\langle l(\tau) \rangle_0 \propto \bar{l}\tau^{1/2} \sim N - l_0 , \tag{39}$$

i.e., until the mean distance of travel is of the order of the distance from the source of carrier to the distant boundary of the sample. Hence, the integral in Eq. (34) makes little contribution until $\tau \sim \beta^2$.

After inserting Eq. (37) into (34), multiplying by l and summing, one has

$$\langle l(\tau) \rangle \equiv \sum_{l=1}^{N} l\tilde{P}(l,t) = l_0 + \langle l(\tau) \rangle_0 - \int_0^\tau d\tau' \tilde{F}(N-l_0,\tau') \langle l(\tau-\tau') \rangle_0 \tag{40a}$$

$$= l_0 + \langle l(\tau) \rangle_0 - \frac{\beta\bar{l}}{\pi} \int_0^\tau d\tau' \tau'^{-3/2} \times e^{-\beta^2/\tau'} (\tau-\tau')^{1/2} . \tag{40b}$$

The integral in Eq. (40b) can be transformed to

$$\frac{\beta\bar{l}}{\pi} e^{-\beta^2/\tau} \int_0^\infty \frac{dy\, y^{1/2}}{y+1} e^{-(\beta^2/\tau)y} = (\beta\bar{l}/\pi^{1/2}) e^{-\beta^2/\tau} [\beta^{-1}\tau^{1/2} - \pi^{1/2} e^{\beta^2/\tau} \operatorname{erfc}(\beta/\tau^{1/2})] , \tag{41}$$

where we have used Formula 2.1.2 of Ref. 17. One now has

$$\langle l \rangle = l_0 + \bar{l}\,(\tau/\pi)^{1/2}(1 - e^{-\beta^2/\tau}) + \beta\bar{l} \operatorname{erfc}(\beta/\tau^{1/2}), \tag{42}$$

which at early and late times has the asymptotic expressions

$$\langle l \rangle \sim \begin{cases} l_0 + \bar{l}\,(\tau/\pi)^{1/2} + \dots , & \beta/\tau^{1/2} > 1, \\ N - \bar{l}\,\beta^2(\tau\pi)^{-1/2} + \dots , & \beta/\tau^{1/2} < 1. \end{cases} \tag{43}$$

In the early-time regime, $\langle l \rangle \simeq \langle l(\tau) \rangle_0$, while as $\tau \to \infty$, $\langle l \rangle \to N$, the thickness of the sample. It is more revealing to examine the current

$$I(t) \propto \frac{d\langle l \rangle}{d\tau} = \tfrac{1}{2}\bar{l}\,(\pi\tau)^{-1/2}(1 - e^{-\beta^2/\tau}). \tag{44}$$

At early times, when $\beta/\tau^{1/2} \gg 1$, the current is just the unperturbed value (28b) of an infinite medium. For $\beta/\tau^{1/2} \ll 1$, the expansion of the exponential yields

$$I(t) \propto (\bar{l}\,\beta^2/2\pi^{1/2})\tau^{-3/2}. \tag{45}$$

Thus the dominant influence of the absorbing boundary on the current is to decrease its magnitude sharply after some characteristic time. The general behavior of the current is most clearly evident in a $\log I$-$\log \tau$ plot of the expression in Eq. (44) shown in Fig. 15. A characteristic time t_τ can easily be obtained from the change in slope in Fig. 15, with

$$\tau_t \simeq [(N-l_0)/\bar{l}\,]^2 \tag{46}$$

($\tau_t \equiv W_M t_\tau$). The change of slope is also shown in Fig. 7, and it is to be emphasized that the t_τ defined in this manner is not the same as the one associated with the plateau, discussed in Sec. I. The fraction of carriers which have survived until time τ, $S(\tau)$, can be determined

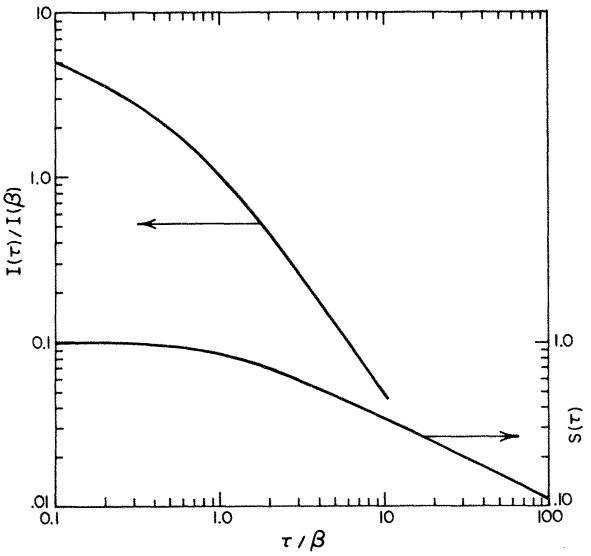

FIG. 15. Plot of Eq. (44) for the current $I(\tau)$ derived from an analytic solution to the random walk governed by $\psi_2(t)$ in the presence of an absorbing boundary. The lower curve is the fraction of surviving carriers $S(\tau)$ as a function of time in units of the transit time $\beta \equiv (N-l_0)/\bar{l}$.

by summing (24) from 1 to N. If one uses the identity

$$\sum_{l=1}^{N} G(l-l_0, t) = 1 \tag{47}$$

to obtain

$$S(\tau) \equiv \sum_{l=1}^{N} \tilde{P}(l, \tau) = 1 - \int_0^{\tau} d\tau' \tilde{F}(N-l_0, \tau')/W_M$$
$$= 1 - \beta\pi^{-1/2} \int_0^{\tau} dx\, x^{-3/2} e^{-\beta^2/x} = \mathrm{erf}(\beta/\tau^{1/2}). \tag{48}$$

This expression could also have been obtained from Eq. (35) by setting $k=0$. The explicit form for this appears in Eq. (B14), with the term proportional to κ^{-l_0} omitted. At the transit time τ_t, the fraction of survivors is

$$S(\tau_t) = \mathrm{erf}\,(1) = 0.84. \tag{49}$$

The time τ_x at which the fraction has declined to 0.5 is $\tau_x/\tau_t = 4.3$. We exhibit a log-log plot of $S(\tau)$ in Fig. 15.

With the choice $\psi_2(t)$, we have demonstrated the basic behavior of a packet of carriers drifting towards an absorbing boundary under the influence of a field. Now $\psi_2(t)$ is a representative of the class (31) that can be expected to prevail for the time regime $\tau \sim \tau_t$ of the duration of transport experiments of disordered material (cf. Sec. 3).

In the general case (31), a simple closed-form expression for $\langle l \rangle$ does not seem to exist, except for some specific values such as $\alpha = \frac{1}{2}$, $\frac{1}{3}$, etc. However, its asymptotic behavior can be derived from that of the first passage-time distribution function $\tilde{F}(N-l_0, \tau)$. We have studied this function through its Laplace transform in Appendix C and found, for $0 < \alpha < 1$,

$$\tilde{F}(N-l_0, \tau)/W_M \sim \frac{\exp\{-[(1-\alpha)/\alpha](\alpha b/\tau^{\alpha})^{1/(1-\alpha)}\} h(\tau)}{\tau[2\pi(1-\alpha)(\tau^{\alpha}/\alpha b)^{1/(1-\alpha)}]^{1/2}}, \tag{50}$$

where

$$h(\tau) \sim \begin{cases} 1, & b/\tau^{\alpha} \gg 1 \\ \tau^{-(1-\alpha/2)/(1-\alpha)}, & b/\tau^{\alpha} \ll 1 . \end{cases} \tag{51}$$

The calculation for $\langle l(\tau) \rangle$ based on Eqs. (40a), (32), (50), and an interpolation formula for $h(\tau)$, will be carried out elsewhere. However, in the long-time limit $\beta/\tau^{\alpha} \ll 1$, Shlesinger[16] has carried out the computation with the use of Tauberian theorems; a review of his work is included in Appendix A. We shall illustrate the content of these theorems by considering a contour-integral expression of $I(t)$. The procedure is as follows: one represents $d[\Sigma l \tilde{P}(l, t)]/d\tau$ in terms of the Laplace transform of Eq. (34) [cf. Eqs. (152-162) of Ref. 15],

$$I(t) = \frac{1}{2\pi i} \int_{c-i\infty}^{c+i\infty} d\tau\, e^{s\tau} \tilde{I}(s), \tag{52a}$$

$$\tilde{I}(s) \propto [1-\psi^*(s)] \left[\sum l G(l-l_0, \psi^*) - \left(\frac{G(N-l_0, \psi^*)}{G(0, \psi^*)} \right) \sum l G(l, \psi^*) \right], \tag{52b}$$

where s is the dimensionless Laplace-transform variable, $s \equiv u/W_M$. The ratio of the two G functions in Eq. (52b) is just the Laplace transform of $\tilde{F}(N-l_0, \tau)$. For $\tau \gg 1$, one must consider the $s \ll 1$ limit of $\tilde{I}(s)$ in Eq. (52b). Using Eqs. (B6), (B7), and

$$\epsilon \equiv [1-\psi^*(s)]/\bar{l} \underset{s \ll 1}{\rightarrow} cs^{\alpha}/\bar{l} \tag{53}$$

[from Eq. (155) of Ref. 15], one can obtain

$$\tilde{I}(s) \sim (1 - e^{-(N-l_0)\epsilon})/\epsilon, \tag{54}$$

where we have retained the leading singular terms of Eq. (52b). Inserting Eq. (54) into (52a), we proceed in the same manner as we did in Appendix C for the asymptotic development of $\tilde{F}(N-l_0, \tau)$ for $\beta/\tau^{\alpha} \ll 1$. The contour of Eq. (52a) is displaced, as in Fig. 16, to C, encircling the branch point of $\tilde{I}(s)$. Corresponding to the two time regimes discussed above, one has

$$I(t)\propto\begin{cases}\dfrac{\bar{l}}{2\pi i}\displaystyle\int_C \frac{ds\,e^{s\tau}}{cs^{\alpha}}=\frac{\bar{l}}{c\Gamma(\alpha)\tau^{1-\alpha}}, & (N-l_0)\epsilon\gg 1 \qquad (55a)\\ \dfrac{\bar{l}}{2\pi i}\displaystyle\int_C ds\,e^{s\tau}\left[\frac{N-l_0}{\bar{l}}-\frac{1}{2}\left(\frac{N-l_0}{\bar{l}}\right)^2 cs^{\alpha}+\cdots\right]=\tfrac{1}{2}\bar{l}\left(\frac{N-l_0}{\bar{l}}\right)^2\frac{c}{[-\Gamma(-\alpha)\tau^{1+\alpha}]}, & (N-l_0)\epsilon\ll 1, \qquad (55b)\end{cases}$$

where only terms containing branch points contribute to the integral evaluated on C. Thus, from a mathematical point of view, the effect of the absorbing boundary is to cause a "time-dependent" transition in the branch point ($s^{-\alpha}\to s^{\alpha}$) in the Laplace transform of $I(t)$. Equations (55a) and (55b) were first obtained by Shlesinger using Tauberian theorems (cf. Appendix A). The time dependence of $I(t)$ for a $\psi(t)\propto t^{-(1+\alpha)}$ is shown schematically in Fig. 7. One observes that it is a generalization of the behavior shown in Fig. 15 for the special case $\alpha=\frac{1}{2}$. It is schematic in the sense that one does not have a closed expression like Eq. (44) but knows that $I(t)$ undergoes a transition, as indicated in Eqs. (55a) and (55b), from $\tau^{-(1-\alpha)}\to\tau^{-(1+\alpha)}$, as β/τ^{α} goes through unity with increasing τ. One notes that the slopes of the $\log I$-$\log\tau$ plot sum to -2. This can be considered a crucial test of our model when experimental data are being analyzed.[18] Furthermore, the fact that the transit time τ_t varies as $\beta^{1/\alpha}$ will be shown to have considerable significance.

III. DISCUSSION OF RESULTS AND CONCLUSIONS

The traditional macroscopic description of carrier transport is associated with the central-limit theorem of probability. The total displacement of a carrier in a biasing field is considered to be a succession of independent displacements such that the time intervals between the initiation of successive displacements, which we call hopping times, have a narrow distribution function, as do the lengths of the individual displacements. The small dispersions in these two distributions imply that an initially narrow carrier packet remains narrow as it traverses the sample. The spatial distribution of the packet becomes Gaussian with increasing time, while spreading becomes negligible compared with the distance traversed; the velocity of propagation of the packet becomes constant. Thus, a clearly defined transit time proportional to the thickness of the sample appears naturally in this traditional description. As noted earlier, however, observations on charge-carrier mobility in some insulators seem to violate this description.

We have introduced in Sec. II a new stochastic model in which we relaxed the hypothesis of a small dispersion in the hopping-time distribution function $\psi(t)$. A small dispersion in hopping times would imply that the duration of the experiment t_τ is large compared to a characteristic time for an individual hop, e.g., the mean hopping time $\bar{t}$. For a carrier hopping across an amorphous insulating film, this does not seem to be the case. The introduction of a long tail in $\psi(t)$ such that

$$\psi(t)\sim\text{const}\times t^{-(1+\alpha)},\quad t=O(t_\tau) \qquad (56)$$

with $0<\alpha<1$, yields an anomalous non-Gaussian transport which, as has been seen, has properties consistent with experimental measurements on two diverse systems, As_2Se_3,[8,9] and TNF-PVK.[11] If $\psi(t)$ satisfies Eq. (56) for all $t_0<t<\infty$ (where t_0 is some arbitrarily chosen time), then $\bar{t}=\infty$. However, as emphasized in Eq. (56), the algebraic tail of $\psi(t)$ is operative for the restricted time range of the experiment. We shall discuss this point more completely, below. By using the distribution Eq. (56) to calculate the packet propagator $P(l,t)$, we have shown that the mean position of a carrier in the packet is given at time t by

$$\langle l\rangle\propto t^{\alpha},\quad 0<\alpha<1, \qquad (57)$$

and that the ratio of the dispersion of the packet to its mean position is independent of the time,

$$\sigma/\langle l\rangle=\text{const}. \qquad (58)$$

The current $I(t)$ associated with such a moving packet exhibits the time dependence of Fig. 7, with

$$I(t)\propto\begin{cases}t^{-(1-\alpha)}, & \langle l\rangle\ll L\\ t^{-(1+\alpha)}, & \langle l\rangle\gtrsim L\,.\end{cases} \qquad (59)$$

We now discuss experiments reported in Refs. 8, 9, and 11, on the basis of Eqs. (57)–(59), and present a justification of the employment of Eq. (56).

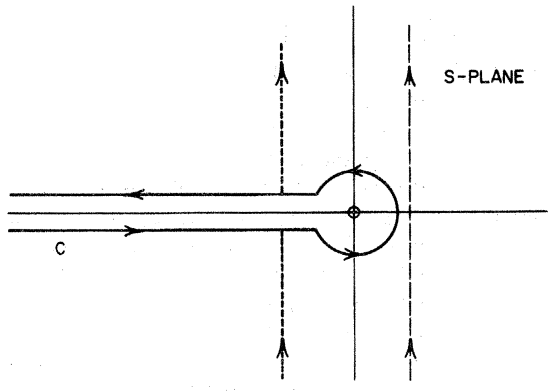

FIG. 16. Integration contours in the complex s-plane used for the computation of the current $I(t)$ (cf. text).

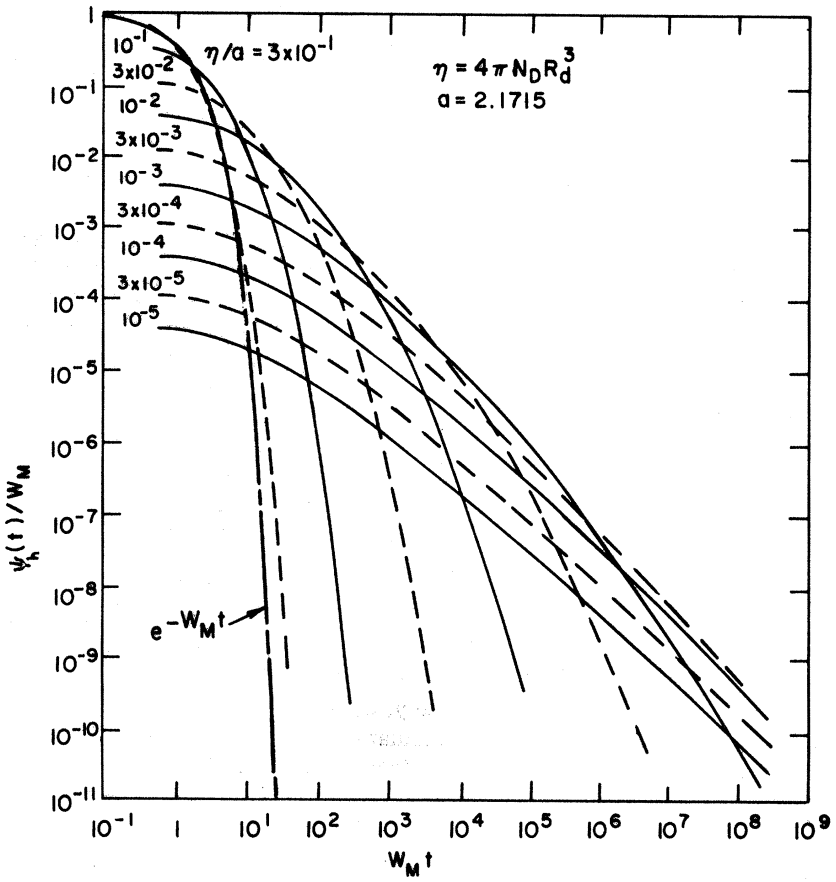

FIG. 17. Hopping-time distribution function $\psi_h(t)$ calculated for a random medium (Ref. 14). The parameter η is a dimensionless measure of the localized site density. The broken line curve (—— - ——) is $\psi_h(t)/W_M = \exp(-W_M t)$.

A first-principles calculation of $\psi(t)$ for hopping through a random medium has been considered in Ref. 14. We outline the procedure in Appendix D and reproduce the results in Fig. 17. We designate that choice of $\psi(t)$ by $\psi_h(t)$. The reduced $\psi_h(t)/W_M$ is a function of two dimensionless variables, $\tau \equiv W_M t$, $\eta \equiv 4\pi N_D R_d^3$, where N_D is the density of localized sites for hopping carriers, and R_d is the charge-localization radius (one-half the effective Bohr radius). The function $\psi_h(t)$ is related to an ensemble average of the probability of hopping between sites. It is a direct measure of the degree of fluctuation of this probability. In the computation of $\psi_h(t)$, only positional disorder of the localized sites has been considered. The temperature dependence is contained in $W_M \propto e^{-\Delta/kT}$, where Δ is an average hopping activation energy. The transition rate $W(\vec{r}) = W_M e^{-r/R_d}$. If one includes fluctuations in Δ, then $\psi_h(t)$ would depend on an additional variable,[19] Δ_0/kT, where Δ_0 is a measure of the dispersion of Δ. If there is no disorder, only one site-to-site transition rate $W(\vec{r}) = W$ exists, and $\psi_h(t)/W = e^{-Wt}$. As η increases, the dispersion in the transition rate decreases, and $\psi_h(t)$ approaches a limit, the exponential function. Conversely, as η decreases, the dispersion in the transition rate increases, and $\psi_h(t)$ approaches a function which for large t has an inverse-power decline. The long tail of $\psi(t)$ can be understood as follows: With a wide range of $W(\vec{r})$, one can always find a pair of sites corresponding to a specified hopping time τ; with a single W, a cutoff W^{-1} exists; τ is either less than or greater than the hopping time W^{-1}.

More precisely, in Fig. 17,

$$\psi_h(t)/W_M = \eta(\ln\tau)^2/\tau^{1+(\eta/3)(\ln\tau)^2} . \tag{60}$$

In calculating an ac conductivity $\sigma(\omega)$ for hopping motion when the frequency ω is varied over many decades, one must use the expression for $\psi_h(t)$ in Eq. (60), especially when one encompasses the $\sigma(\omega)$ range from the ω^s region to the dc limit.[14] However, for a t_τ measurement, one can approximate $\psi_h(t)$ by Eq. (56) where

$$\alpha \simeq \tfrac{1}{3}\eta(\ln\tau)^2, \quad \tau = O(\tau_t), \quad \tau_t \gg 1. \tag{61}$$

This approximation increases the mathematical tractability of our model.

Thus, the physical justification for the use of Eq. (56) is that the time dependence of $\psi_h(t)$, calculated for a spectrum of $W(\vec{r})$ appropriate for a random medium, is simulated by $t^{-(1+\alpha)}$ for $t \simeq t_\tau$. Here,

α is a function of η, W_M, and t_τ. However, in contrast to Eq. (56), $\psi_h(t)$ has a finite first moment,

$$\bar{\tau} = (\pi\eta^{-1/2})^{1/2} \exp(\tfrac{2}{3}\eta^{-1/2}) . \tag{62}$$

If one used $\psi_h(t)$ in the computation of $\tilde{P}(l, t)$, *then the carrier packet would approximate a Gaussian shape in the range* $\tau_t \gg \bar{\tau}$. This fact emphasizes our point that the unusual results [Eqs. (57)–(59)] derived from the stochastic (hopping) process are not so much due to a difference in genre, as they are to a crucial interaction between the *conditions of the experiment determining* τ_t (i.e., E, L) and the *parameters of the system determining* $\bar{\tau}$ (i.e., N_D, R_d).

To stress that the non-Gaussian results are not due merely to a sampling of a small number of events (a few hops per transit), one must have $\tau_t > \tau_{1/2}$. The (median) time $\tau_{1/2}$ is defined to be the time (after arrival) at which the probability of a carrier remaining on the site of arrival is equal to $\frac{1}{2}$. One summarizes the above discussion with the constraint

$$\tau_{1/2} \ll \tau_t \lesssim \bar{\tau} . \tag{63}$$

For $\psi_h(t)$,

$$\tau_{1/2} = \exp(3\ln 2/\eta)^{1/3} , \tag{64}$$

and one has, for a value $\eta = 10^{-3}$,

$$\bar{\tau} = 1.42 \times 10^{10},$$

$$\tau_{1/2} = 3 \times 10^{5} , \tag{65}$$

a difference between these characteristic times of almost five orders of magnitude!

As discussed in Sec. I the surprising element in the results of the transient photocurrent measurement [Fig. 1(b)] in an increasing number of amorphous insulators is not the long tail (Fig. 3), which indicates some sort of dispersion in transit times, but the universality in the shape of $I(t)$ over a wide range of t_τ (Fig. 4). This universal current trace $I(t)/I(t_\tau)$ vs t/t_τ was first quantitatively demonstrated by Scharfe[9] in his measurements on a-As_2Se_3. Another remarkable aspect of this dispersed transport, analyzed by Scharfe, can be seen in a log-log plot of t_τ^{-1} vs E/L. All the inverse transit times for a considerable range of both field and *sample thickness* lie on one straight line, with a slope $\simeq 2$, i.e., $\tau_\tau^{-1} \propto (E/L)^2$. By relating t_τ to the effective drift mobility in the conventional way, with the use of Eq. (2), one would obtain

$$\mu \propto E/L . \tag{66}$$

A field-dependent μ has become a familiar object in the phenomenology of insulating materials, but a carrier drift mobility that depends upon sample thickness is most unusual!

The actual choice of t_τ has depended on discerning some plateau in the trace of $I(t)$—a residue of the idealized current shape shown in Fig. 2. However, quite a number of current traces on As_2Se_3 and some polymeric films display a completely featureless time decay. Moreover, the presence or absence of a small plateau is often a function of the immediate sample history, e.g., the number and frequency of incident light flashes and the degree of dark resting of the sample. A more revealing analysis of these featureless traces is obtained[18] with a log-log plot $I(t)/I(t_\tau)$ vs t/t_τ on As_2Se_3 made by Pfister[9] in connection with his study of the pressure dependence of t_τ (Fig. 5). The data (including one set at high pressure) exhibit a universality in the current shape over three-orders-of-magnitude range in t_τ. The data clearly show two slopes, each persisting for over an order of magnitude in t. The time dependence of $I(t)$ corresponds to $t^{-0.55}$ with a transition to $t^{-1.45}$. This behavior is in complete comformity with the theoretical results [Eq. (57) and Fig. 7] for $\alpha = 0.45$. The solid line in Fig. 5 is derived from the analytic result for $\alpha = \frac{1}{2}$ (Fig. 15, slightly "tilted" to accomodate the small change in α, computed in Sec. II and Appendix B). For general α, one can determine the two slopes [cf. Eq. (57)] and estimate from Eq. (C12) the time dependence of the transition region. However, in the case of $\alpha = \frac{1}{2}$, one can derive an analytic expression Eq. (44) for $I(t)$ covering the entire range of t.

The solid line is in excellent agreement with the experimental data. As detailed in Sec. II, the change in slope for the log-log plot of $I(t)$ corresponds to the carriers encountering the oppositely charged electrode (the absorbing barrier). The transit time is associated with this change, i.e., the step change in the quantity $-d[\ln I(t)]/d(\ln t)$.

In Fig. 18 we show traces of both a continuous recording of an electronically produced $\log I$-$\log t$ and a photograph of the linear $I(t)$ vs t displayed on a cathode-ray tube. The time designated as t_τ is marked with an arrow on both traces. The transit time is defined by the $\log I$-$\log t$ plot. The corresponding time on the $I(t)$ plot is an undistinguished point on a completely featureless curve. A convenient choice for t_τ is the time defined by the intersection of the extrapolated lines of constant slope (dashed lines in Fig. 18). For $\alpha = \frac{1}{2}$, this point is

$$\tau_t^{1/2} = 0.92(N - l_0)/\tilde{l} \simeq 0.92L/\tilde{l}\rho , \tag{67}$$

where ρ is the average intersite separation. The theoretical curve for $\alpha = 0.45$ is but slightly modified, so we take

$$\tau_t^{0.45} = 0.95L/\tilde{l}\rho . \tag{68}$$

There are As_2Se_3 samples that exhibit another value of α, and Pfister encountered materials problems connected with thin samples ($L < 30$ μm); these

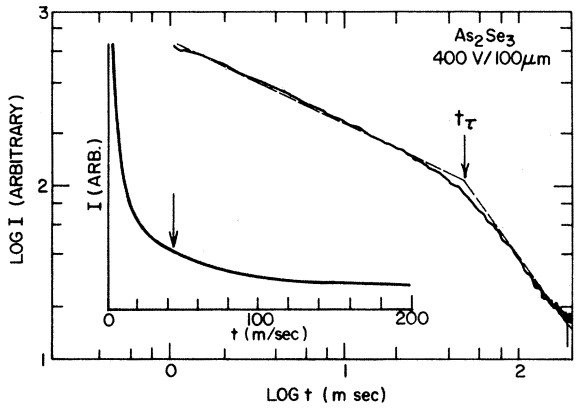

FIG. 18. Trace of an electronically produced log I - log t plot for As_2Se_3 measured by Pfister. The dashed lines have slopes of -0.55 and -1.45, respectively. The intersection of the lines is denoted as t_τ. The same t_τ is indicated on the trace of the oscillogram of I vs. t in the inset.

will be discussed in another work.

The dependence on the electric field E is contained in $\bar{l}$, which is equal to $2p[2\tilde{\eta}(E)-1]$. The parameter $\tilde{\eta}$ is a measure of the spatial asymmetry introduced by E in the transition rates between the sites. Moreover, $\tilde{\eta}(E)$ can be a general (nonlinear) function of E. The exact form of $\tilde{\eta}$ for any specific system must be determined by a first-principles calculation of the transition rates, which in turn depends on a knowledge of the effect of an electric field on the site wave functions and site energy levels or intersite barrier.

One can make a prediction of the sample thickness dependence of τ_t independently of $\tilde{\eta}(E)$,

$$\tau_t = cL^{1/\alpha}/(\bar{l}\rho)^{1/\alpha}, \tag{69}$$

where c is a numerical constant of order unity. In the case of As_2Se_3, from Eq. (68), one has $1/\alpha = 2.2$, $c = 0.89$, and

$$\tau_t \propto L^{2.2}. \tag{70}$$

Hence, *for fixed* E, a current trace of the form in Figs. 5 and 18, *must* correspond to the L dependence in Eq. (70). In Fig. 19 we exhibit a log-log plot of t_τ vs L for a range of L varying from 31 to 100 μm. The values of the transit time have all been determined by the intersection of the lines with slopes -0.55 and -1.45 and at a field of 10^5 V/cm. The slope of the solid line through the data points is equal to 2.2, in excellent agreement with Eq. (70). Thus, the anomaly of a thickness-dependent mobility, as discussed in Eq. (66), is resolved. The apparent L dependence of μ is related to the propagation characteristics of the carrier packet.

The conventional relation Eq. (2) is based on the assumption that the mean position $\langle l \rangle$ of the carriers changes linearly in time. Expression (57) for $\langle l \rangle$ requires a *time-dependent mobility* to interpret the transit-time measurements in the usual way with Eq. (2). Therefore, the insistence on the use of a mobility μ to describe the packet motion implies that μ depends on any parameters, such as L and E, that change the time scale of the measurement.

Let us consider the nature of the field dependence. First, we must estimate $\tilde{\eta}(E)$. Since we have little information of the nature of the localized states in As_2Se_3, we shall make the simplest assumptions possible. By postulating a field-independent mobility, we write

$$2\tilde{\eta}(E) - 1 \propto E, \tag{71}$$

the asymmetry being linear in E. Inserting Eq. (71) into (69), one has

$$\tau_t \propto (L/E)^{2.2}. \tag{72}$$

In Fig. 20 we show a log-log plot of t_τ^{-1} vs E/L. The range of transit time covers four orders of magnitude and is a composite of varying both L and E. The slope of the solid line is equal to 2.2, in agreement with Eq. (72). Thus the apparent

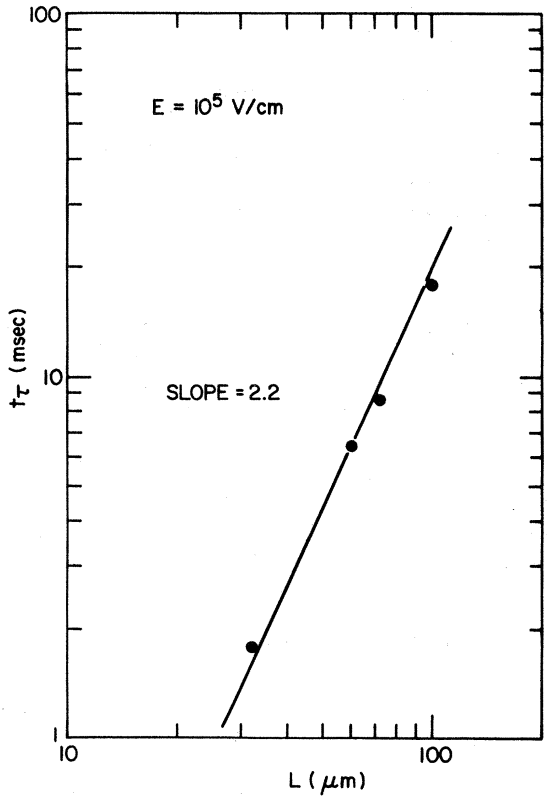

FIG. 19. Log-log plot of the transit time t_τ vs L. The solid line of slope 2.2 is the theoretical curve.

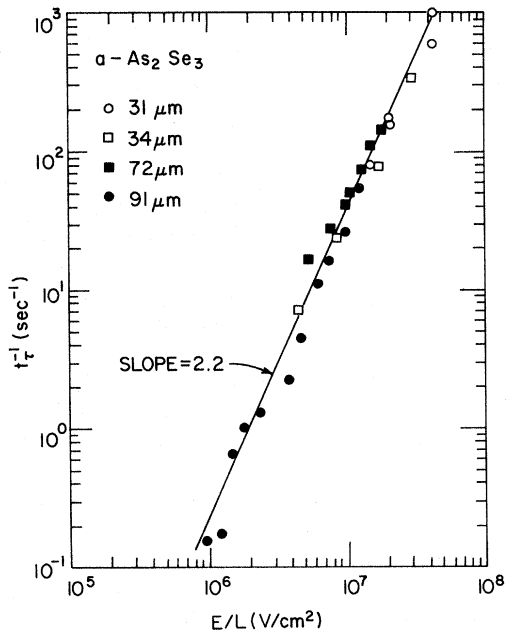

FIG. 20. Log-log plot of the inverse transit time t_τ^{-1} vs E/L. The solid line of slope 2.2 is the theoretical curve.

field dependence of the mobility appears on the same basis as the thickness dependence, the field being another parameter that changes the time scale of the experiment. It will be shown below that field-dependent mobilities in other systems cannot be explained entirely on this basis.

To determine the various physical parameters in As_2Se_3 we proceed in a self-consistent manner. With the lowest field that Pfister used in his measurements, we set

$$2\tilde{\eta}(E) - 1 \lesssim 0.1 . \tag{73}$$

To obtain τ_t we choose a value of ρ in Eq. (68) and determine if the magnitude of τ_t is then consistent with this ρ via the constraint imposed by the relation in Eq. (61) $[\eta \equiv \frac{3}{8}(a_B/\rho)^3]$. Let $N_D = 1.5\times 10^{17}$ cm^{-3}, corresponding to $\rho = 1.17\times 10^{-6}$ cm, and, with Eq. (68), we have $\tau_t = 5.7\times 10^{11}$ ($L = 91$ μm). Inserting this value for τ in Eq. (61), we determine $\eta = 1.8\times 10^{-3}$ for $\alpha = 0.45$. Therefore, for this low field ($t_\tau = 6.6$ sec), we have the following (self-consistent) parameters for As_2Se_3:

$$N_D = 1.5\times 10^{17}\ \text{cm}^{-3},\quad a_B = 19.7\ \text{Å},\quad W_M \lesssim 5\times 10^{10}\ \text{sec}^{-1}. \tag{74}$$

The values of N_D and a_B in Eq. (74) are very reasonable. They are close to the values $N_{1oc} = 10^{17}$ cm^{-3}, and $\frac{1}{2}a_B = 10$ Å, determined for a-Ge.[20]

One can view the present theory as a one-parameter model. We choose the value of α to fit the tail of $I(t)$. This choice then predicts *two independent* aspects of the transport, the initial time dependence of $I(t)$ $[I(t) \propto t^{-(1-\alpha)}]$ and the dependence of τ_t on L and E, as in Eq. (69). The determination in Eq. (74) of a reasonable set of physical parameters in As_2Se_3, based on $\psi_h(t)$ as the physical justification for the use of a $\psi(t) \propto t^{-(1+\alpha)}$, adds to the hopping model of the transport. The parameters specified in Eq. (74) imply that the lower bound for the average number of hops required to transverse the 91-μm sample is $L/\rho \simeq 8\times 10^3$. This large number hardly corresponds to a case of "small statistics."

There are systems, TNF-PVK mixtures, in which one has independent knowledge of a hopping transport and of some of the pertinent parameters such as N_D and a_B. We shall now analyze the measurements of Gill[11] on those systems.

By varying the relative composition of the TNF monomer in the polymer PVK, Gill was able to demonstrate that the electron mobility μ_e has an exponential dependence on the average separation of the TNF molecules,

$$\mu_e \propto R_{\text{TNF}}^2 \exp(-R_{\text{TNF}}/R_0), \tag{75}$$

where

$$R_0 = 0.9\ \text{Å}. \tag{76}$$

Gill also found a similar dependence of the hole mobility on the separation of the uncomplexed vinylcarbazole units. Relation (75) is good evidence for a hopping mechanism. Moreover, by varying the composition, Gill established the TNF monomer as the hopping site for electrons. By equating R_d and R_0, one now has knowledge of two important parameters N_D and R_d ($\equiv \frac{1}{2}a_B$). In Fig. 6 we reproduce a log-log plot of Gill's data for $I(t)$, for 1:1 molar ratio of TNF-PVK, as presented in a recent paper by Seki.[21] One notes again the universal shape of $I(t)$. The transit-time range in Fig. 6, however, extends over only one order of magnitude. The sum of the slopes of the solid lines through data points in Fig. 6, -0.2 and -1.8, again equal to -2.0, in excellent agreement with the theoretical prediction (59) for $\alpha = 0.8$. For this higher value of α, one observes a more rapid transition between the asymptotic slope lines (as compared to Fig. 5 for $\alpha = 0.45$), in agreement with the time dependence in (C12). Now, $\alpha = 0.8$ corresponds to

$$\tau_t \propto L^{1.25}, \tag{77}$$

which is a nearly linear dependence on thickness, in agreement with reported results.[11]

In contrast to As_2Se_3, one can calculate $\eta(\equiv 4\pi N_D R_d^3)$, *a priori*, for TNF-PVK. One obtains $\eta \simeq 10^{-2}$ for the 1:1 molar ratio with $N_D = N_{\text{TNF}} \simeq 10^{21}$ cm^{-3} and $R_d \simeq 0.9$ Å, where N_{TNF} is the concentration of complexed TNF.[22] Using this value

of η in Eq. (61) and $\alpha = 0.8$, one determines that the range of τ for the transit time is

$$1{:}1\ \text{TNF-PVK},\quad \tau_t \simeq 5\times 10^6. \tag{78}$$

The magnitude of τ_t in Eq. (78) will now be shown to be consistent with that obtained with the use of Eq. (69). For $L = 5$ μm and $\rho = 6.2$ Å (corresponding to $N_{\mathrm{TNF}} = 10^{21}$) one has

$$\tau_t = \left(\frac{2.4\times 10^4}{2\tilde{\eta}(E) - 1}\right)^{1.25}. \tag{79}$$

With a nominal value of $2\tilde{\eta}(E) - 1 \approx 0.1$ in Eq. (79), one obtains $\tau_t \simeq 5\times 10^6$, in good agreement with the value in Eq. (78)

To rephrase the above numerical argument, we have for TNF-PVK only one unknown physical parameter of the hopping model, namely, W_M, $(\equiv W_0\, e^{-\Delta/\kappa T})$, the prefactor of the intersite transition rate. Inserting the experimental values for N_D and R_d, one must satisfy two independent constraints, Eqs. (61) and (69), for the value of W_M. We have obtained a value for W_M that does satisfy both! The transit time measured by Gill for $L = 5$ μm and $E = 5\times 10^5$ V/cm $[2\tilde{\eta}(E) - 1 \simeq 0.1$ used above is assumed to correspond to this field value] is $t_\tau = 2.0$ msec. Hence for $\tau_t \simeq 4\times 10^6$, one has

$$W_M = 2.5\times 10^9\ \mathrm{sec}^{-1}. \tag{80}$$

The smaller value of W_M for TNF-PVK in Eq. (80) compared to W_M for As_2Se_3 in Eqs. (74) is consistent with the larger activation energy for TNF,

$$\Delta_{\mathrm{TNF}} \simeq 0.65\ \mathrm{eV},\quad \Delta_{\mathrm{As_2Se_3}} \simeq 0.5\ \mathrm{eV}. \tag{81}$$

In contrast to As_2Se_3, the effective mobility in TNF-PVK appears to be field-dependent. Gill has used a field dependence of the form

$$\mu = \mu_0 \exp[-(\Delta - \beta E^{1/2})/\kappa T_{\mathrm{eff}}]. \tag{82}$$

The strongest evidence for Eq. (82) is contained in Fig. 7 of Ref. 11, a plot of the activation energy of μ, E_a vs $E^{1/2}$. We stress this point because Eq. (82) in general would indicate a very rapid field dependence for $\mu(E)$. However, over the available limited mobility range shown in Fig. 4 of Ref. 11, the field dependence of $\mu(E)$ is quite mild and could be fit with an algebraic dependence $\mu(E) \propto E^{1.3}$. We are not seriously suggesting that this is the case. However, we wish to emphasize that, although the form of $\mu(E)$ in Eq. (82) does imply a very rapid field dependence for μ, this has not been experimentally established, whereby μ changes by orders of magnitude over some field range. Nonetheless, with $\alpha = 0.8$, one would predict an effective $\mu \propto E^{0.25}$ if one assumed no intrinsic $\mu(E)$ (i.e., the asymmetry linear in E as for As_2Se_3). This is clearly not the case and one needs, *at least*, $2\tilde{\eta}(E) - 1 \propto E^{1.8}$ over the experimental range of E.

To consider the field dependence from a more fundamental approach, one would have to calculate the effect of the field on the transition rates $[W(\vec{r})]$ and then incorporate these effects into a calculation of $\psi(s, t)$,[14,19] the probability rate of hopping a distance $\vec{s}$ in a time t. We reserve this approach for another investigation. A few remarks may, however, be in order. There is some difficulty in understanding the magnitude of the activation energies in (81) purely on the basis of the idea that Δ represents the width of the energy dispersion of the localized levels[21] (the disorder energy). One can conjecture that Δ consists of two parts, a self-trapping or small-polaron part Δ_p and the disorder-energy part Δ_d. In single-crystal sulfur,[4] there is transport evidence that the electron propagates as a small polaron, but the Δ_p is independent of electrical field. Thus, a reasonable hypothesis, which will be explored in future work, is that the E dependence is entirely in Δ_d.

In summary, the stochastic transport model has enabled us to understand the nature of the transient photoconductivity in at least two different amorphous systems, one inorganic (As_2Se_3) and the other organic (TNF-PVK).

First, one has been able to understand a current-trace shape as shown in Fig. 18. There is no "flat part," characteristic of the idealized current response shown in Fig. 2, to specify a transit time. $I(t)$ traces, such as obtained in Fig. 18, were formerly "unanalyzable." By transposing such an $I(t)$ to a log-log plot, the transit time is indicated by the region where $-d[\ln I(t)]/d(\ln t)$ experiences a step change. Furthermore, with the log-log display of the current, in both As_2Se_3 and TNF-PVK, the theory has accounted for the overall general shape and, in fact, for the detailed time dependence with the appropriate choice of one parameter α. Whatever the choice of α $(0 < \alpha < 1)$, the theory predicts that the slopes of the lines, on the log-log plot, should sum to -2.0. There is excellent agreement with this firm prediction in Figs. 5, 6, and 18, for *both* As_2Se_3 and TNF-PVK. Thus, with a value of α chosen to fit the tail of $I(t)$, there is an independent prediction of the initial time decay. Moreover, this choice of α must further correlate the shape of $I(t)$ with the thickness dependence of the transit time. For As_2Se_3 with $\alpha = 0.45$, $\tau_t \propto L^{2.2}$, and TNF-PVK with $\alpha = 0.8$, $\tau_t \propto L^{1.25}$, a nearly linear dependence. Both of these correlations have been established experimentally. In the case of As_2Se_3, with an assumption of no *intrinsic* field-dependent mobility, the nonlinear E dependence of τ_t has been understood on the same basis as the L dependence. In the TNF-PVK system, there is now evidence for an intrinsic field dependence of the effective electron (hole) mobility, and the origin of this behavior

will be pursued in a further study.

On a more microscopic level, a set of parameters N_D, R_d, and W_M has been self-consistently determined for As_2Se_3, in conformity with the value of α, using $\psi_h(t)$ as the physical justification for using a $\psi(t) \propto t^{-(1+\alpha)}$. Knowing N_D and R_d for TNF-PVK, one obtained a value of W_M that satisfied two independent constraints (61) and (69) for $\alpha = 0.8$. In addition, the increase of α in 1:1 TNF-PVK relative to As_2Se_3 (i.e., less dispersive transport) can be ascribed to the increase of $N_D R_d^3$ between the two systems.

The next step is to calculate the basic transition rates in the two materials and account for the magnitudes of the parameter W_M.

On a conceptual level, the theory establishes the reason for the universality of $I(t)$ and has shown the limitations of the notion of a mobility in this dispersive type of transport. If one insists on the conventional relation (2) to define an effective μ, then, besides the possibility of an apparent field dependence, one would have to rationalize a thickness dependence of μ! Unless the mean $\langle l \rangle \propto t$, the idea of a μ depending solely on the properties of the material breaks down. For example, if one has $\langle l \rangle \propto t^{\alpha}$, $0 < \alpha < 1$, one could write

$$\langle l \rangle = (V_0/t^{1-\alpha})\, t, \tag{83}$$

and the effective μ would be *time dependent*. Thus, for this type of transport, the present theory relates the transit time to intrinsic-rate processes in the material, but the simple notion of a mobility, field dependent or otherwise, is very limited.

Dispersive transit-time experiments in disordered solids are perhaps only one of a number of physical phenomena in which this very different kind of statistical process, i.e., one that does not obey the central limit theorem, plays a central role.

ACKNOWLEDGMENTS

We wish to thank both M. E. Scharfe and G. Pfister for enlightening discussions about the experiments on As_2Se_3 and the use of unpublished data. We are also indebted to M. Shlesinger for informative discussions on asymptotic properties of random walks and to L. C. Hebel, E. M. Conwell, G. Pfister, R. Zallen, and J. Mort for a critical reading of the manuscript.

APPENDIX A: ASYMPTOTIC DEVELOPMENT OF THE MEAN AND DISPERSION WITH TAUBERIAN THEOREMS

While the asymptotic formulas (29)-(32) were obtained for the specific model characterized by Eqs. (19) and (28), they can immediately be generalized, as recently shown by Shlesinger,[16] through the application of certain Tauberian theorems. It is convenient to characterize the random walk of interest by two functions, the Laplace transform, $\psi^*(u)$, of the waiting-time distribution function (12), and the Fourier component of the probability $\tilde{G}(l, t)$,

$$\gamma(k, t) = \sum_l \tilde{G}(l, t)\, e^{-i\vec{k}\cdot\vec{l}}\,. \tag{A1}$$

Then

$$\gamma(k, t) = \mathfrak{L}^{-1}\left([1 - \psi^*(u)]\{u[1 - \gamma(k)\psi^*(u)]\}^{-1}\right). \tag{A2}$$

Also,

$$\langle l_1(t) \rangle \equiv \sum_l l_1 \tilde{P}(l, t) = \bar{l}\left(\frac{\partial \gamma(k, t)}{\partial \lambda}\right)_{\lambda=1}$$

$$= \bar{l}\,\mathfrak{L}^{-1}\{\psi^*(u)/u[1 - \psi^*(u)]\}\,, \tag{A3}$$

where

$$\bar{l} = \sum l p(l)\,. \tag{A4}$$

Similarly,

$$\sigma^2(t) = \langle l^2 \rangle_{\mathrm{av}} \left(\frac{\partial \gamma}{\partial t}\right)_{\lambda=1} + \bar{l}^2 \left[\frac{\partial^2 \gamma}{\partial \lambda^2} - \left(\frac{\partial \gamma}{\partial \lambda}\right)^2\right]_{\lambda=1}. \tag{A5}$$

When the first two integral moments $\bar{t}$ and $\langle t^2 \rangle_{\mathrm{av}}$ are finite, with

$$\langle t^n \rangle_{\mathrm{av}} \equiv \int_0^{\infty} t^n \psi(t)\, dt\,, \quad \langle l^2 \rangle_{\mathrm{av}} \equiv \sum l^2 p(l)\,, \tag{A6}$$

$$\psi^*(u) = 1 - \bar{t}u + \tfrac{1}{2}u^2 \langle t^2 \rangle_{\mathrm{av}} + \int_0^{\infty} (e^{-ut} - 1 + tu - \tfrac{1}{2}t^2u^2)\, \psi(t)\, dt\,. \tag{A7}$$

The integral contribution can be shown to be $o(u^2)$. Hence

$$\psi^*(u) \sim 1 - \bar{t}u + \tfrac{1}{2}u^2 \langle t^2 \rangle_{\mathrm{av}}\,. \tag{A8}$$

On the other hand, if $\bar{t}$ is infinite and, as $t \to \infty$,

$$\psi(t) \sim [At^{1+\alpha}\Gamma(1 - \alpha)]^{-1} \quad \text{for } 0 < \alpha < 1\,, \tag{A9}$$

Feller[23] has shown that

$$\psi^*(u) \sim 1 - u^{\alpha}/A\,. \tag{A10}$$

An asymptotic expression for $\langle l(t) \rangle$ is obtained from Eqs. (A3), (A8), and (A10), by applying the following Tauberian theorem of Hardy and Littlewood, and Karamata:

If $f(u) \sim Au^{-k}$ as $u \to 0$ with $k > 0$,

then $g(t) \sim At^{k-1}/\Gamma(k)$ as $t \to \infty$ (A11)

when $\mathfrak{L}[g(t)] = f(u)$, A being a constant.

Shlesinger has also used the generalization of this theorem in which A is a slowly varying function of u.

When Eq. (A8) is applicable, we have, from Eqs. (A3), (A8), and (A11), if we set

$$f(u) \equiv \psi^*(u)/u[1 - \psi^*(u)] \sim (\bar{t}u^2)^{-1}\,, \tag{A12}$$

$$g(t) \simeq \langle l(t)\rangle / l \sim t/\bar{t}\,, \tag{A13}$$

which is the classical random-walk result, $\langle l(t)\rangle \sim (\bar{l}/\bar{t})t$.

When Eq. (A9) and (A10) are applicable, the Tauberian theorem implies that

$$f(u) \sim A/u^{\alpha+1} \tag{A14}$$

and

$$\langle l(t)\rangle \sim \bar{l}At^{\alpha}/\Gamma(\alpha+1)\,. \tag{A15}$$

With an absorbing boundary let us consider the Fourier component of $\tilde{P}(l, t)$, $\Gamma(k, t)$, which is related to $\tilde{P}(l, t)$ in the same manner that $\gamma(k, l)$ is related to $\tilde{G}(l, t)$ as given by Eq. (A1). Then

$$\Gamma(k, t) = \gamma(k, t)\, e^{-ikl_0} - \int_0^t dx\, \gamma(k, t-x)\, \tilde{F}(N-l_0, x)\,, \tag{A16}$$

where it is known that

$$\tilde{F}(N-l_0, \tau) = \mathfrak{L}^{-1}\, G(N-l_0, \tilde{\psi}(s))/G(0, \psi(s))\,. \tag{A17}$$

It was shown in Eqs. (158), (138a), and (138b) of Ref. 15 that

$$\frac{G(N-l_0, z)}{G(0, z)} = \frac{\alpha_1^{N-l_0} - (\alpha_1/\alpha_2)^N \alpha_1^{-l_0} + (1-\alpha_1^N)\alpha_2^{-l_0}}{1-(\alpha_1/\alpha_2)^N}$$
$$\sim \alpha_1^{N-l_0} + (1-\alpha_1^N)\alpha_2^{-l_0}\,, \tag{A18}$$

where $|\alpha_2| > 1 > |\alpha_1|$ and

$$\alpha_1 = 1-\epsilon\,, \quad \alpha_2 = [\tilde{\eta}/(1-\tilde{\eta})](1+\alpha_1)\,, \tag{A19}$$

the parameter $\tilde{\eta}$ being related to the bias in the walk as defined by Eq. (28b). Also,

$$\epsilon(z) = (1-z)/2p(2\tilde{\eta}-1)$$
$$+ (1-z)^2[2p(2\tilde{\eta}-1)^2 - \eta]/4p^2(2\tilde{\eta}-1)^3 + O(1-z)^3\,. \tag{A20}$$

Let us again consider the case

$$\psi^*(u) \sim 1 - u^{\alpha}/A_1 + u^{2\alpha}/A_2 - \cdots\,, \tag{A21}$$

for which Eq. (A15) was derived. Then

$$\alpha_1 \sim (u^{\alpha}/A_1 - u^{2\alpha}/A_2 + \cdots)/2p(2\tilde{\eta}-1)\,, \tag{A22}$$

$$\alpha_2 \sim [\tilde{\eta}/(1-\tilde{\eta})][1 + u^{\alpha}/pA_1(2\tilde{\eta}-1) + \cdots]\,. \tag{A23}$$

The Laplace transform of $\Gamma(k, t)$ is, applying the convolution theorem,

$$\mathfrak{L}[\Gamma(k, t)] = \mathfrak{L}[\gamma(k, t)][e^{-ikl_0}$$
$$- G(N-l_0, \tilde{\psi}(u))/G(0, \tilde{\psi}(u))]\,. \tag{A24}$$

Since $\langle l\rangle = i \lim_{k\to 0}(\partial\Gamma/\partial k)$, we find

$$\langle l\rangle = l_0 + \bar{l}\mathfrak{L}^{-1}\{\psi^*(u)/u[1-\psi^*(u)]\}$$
$$\times\{1 - [G(N-l_0, \tilde{\psi}(u))/G(0, \tilde{\psi}(u))]\}\,. \tag{A25}$$

The Tauberian theorems discussed above can be used to find the long-time behavior of $\langle l\rangle$ from the asymptotic properties as $u \to 0$ of the function to the right of the $\mathfrak{L}^{-1}$ operator in Eq. (A25). From Eq. (A18) and (A20), we find that as $u \to 0$,

$$1 - G(N-l_0, \tilde{\psi}(u))/G(0, \tilde{\psi}(u)) \sim 1 - \alpha_1^{N-l_0} - (1-\alpha_1^N)\alpha_2^{-l_0}$$
$$= \epsilon(N-l_0)[1 - \tfrac{1}{2}\epsilon(N-l_0-1)] + \epsilon N[1 - \tfrac{1}{2}\epsilon(N-1)]$$
$$\times[2\eta/(1-\eta)]^{-l_0}(1 + \tfrac{1}{2}\epsilon l_0) + O(\epsilon^3)$$
$$= c_1 u^{\alpha} + c_2 u^{2\alpha} + \cdots\,, \tag{A26}$$

where $c_1, c_2, \ldots$ are numbers which depend on N, l_0, η, and p. We also have

$$\psi^*(u)/u[1-\psi^*(u)] \sim u^{-1-\alpha}A_1[1 + u^{\alpha}(A_1^2 - A_2)/A_1A_2$$
$$+ O(u^{2\alpha})]\,. \tag{A27}$$

The product of Eqs. (A26) and (A27), whose Laplace inverse is required in (A25), is

$$u^{-1}c_1A_1(1 - u^{\alpha}B/c_1A_1 + \cdots)\,, \tag{A28}$$

with

$$B = -[(A_1^2 - A_2)c_1 + c_2A_1A_2]/A_2\,. \tag{A29}$$

Hence, upon application of the Tauberian theorem (A11) we find, as $t \to \infty$,

$$\langle l\rangle \sim l_0 + \bar{l}A_1c_1 - \bar{l}B/t^{\alpha}\Gamma(\alpha+1) + \cdots\,, \tag{A30}$$

and

$$\frac{d\langle l\rangle}{dt} \sim B\bar{l}/t^{\alpha+1}\Gamma(\alpha)\,. \tag{A31}$$

The significance of results (A15) and (A31) are thoroughly discussed in the text.

APPENDIX B: CHARACTERISTIC FUNCTION $\Gamma(k,t)$ FOR $\psi_2(t)$ WITH ABSORBING BOUNDARY

The solution for an absorbing-plane boundary for the asymmetric continuous-time random walk (CTRW) is described in the text [Eq. (34)]. The final form for the propagation is

$$\tilde{P}(l, \tau) = \tilde{G}(l-l_0, \tau) - \int_0^{\tau} d\tau' \tilde{G}(l, \tau-\tau')$$
$$\times \tilde{F}(N-l_0, \tau')/W_M\,, \tag{B1}$$

where $\tau \equiv W_M t$. The characteristic functions are defined as

$$\Gamma(k, \tau) = \sum_{l=1}^{N} e^{-ikl}\tilde{P}(l, \tau)\,, \tag{B2}$$

$$\gamma(k, \tau) = \sum_{l=1}^{N} e^{-ikl}\tilde{G}(l, \tau)\,, \tag{B3}$$

where $k \equiv 2\pi r/N$, r = integer. We substitute the expression for $\tilde{P}(l, \tau)$ in Eq. (B1) into Eq. (B2), and obtain for the characteristic function

$$\Gamma(k, \tau) = \gamma(k, \tau)\, e^{-ikl_0} - \int_0^{\tau} d\tau' \gamma(k, \tau-\tau')$$
$$\times \tilde{F}(N-l_0, \tau')/W_M\,. \tag{B4}$$

For the region of τ of interest in the present paper

($\tau \gg 1$), we can determine $\tilde{F}(N-l_0, \tau)$ from the asymptotic behavior of its Laplace transform

$$\frac{\tilde{F}(N-l_0, \tau)}{W_M} = \frac{1}{2\pi i}\int_{c-i\infty}^{c+i\infty} ds\, e^{s\tau}\, \frac{G(N-l_0, \psi^*(s))}{G(0, \psi^*(s))}\,, \quad \text{(B5)}$$

$$\frac{G(N-l_0, \psi^*(s))}{G(0, \psi^*(s))} \simeq \alpha_1^{N-l_0} + (1-\alpha_1^N)\,\alpha_2^{-l_0}\,, \quad \text{(B6)}$$

where relative contributions of order $(\alpha_1/\alpha_2)^N \simeq \kappa^{-N}$ in Eq. (B6) have been neglected [cf. Eq. (A18)]. [$\kappa \equiv \eta/(1-\eta)$]. The complete expression for $\alpha_{1,2}$ is defined in Eqs. (130) and (128), of Ref. 15 (with $z = \psi^*(s)$]. For $\tau \gg 1$ we only need the form of $\alpha_{1,2}$ for small s,

$$\alpha_1 \simeq e^{-\epsilon}, \quad \alpha_2 \simeq \kappa e^{+\epsilon}\,, \quad \text{(B7)}$$

$$\epsilon \equiv [1-\tilde{\psi}_2(s)]/\bar{l} \simeq 2s^{1/2}/\bar{l}\,. \quad \text{(B8)}$$

Inserting Eqs. (B7) and (B8) into Eq. (B6), we obtain the inverse Laplace transform (using formula 3.2, 14 of Ref. 17)

$$\tilde{F}(N-l_0, \tau)/W_M = [(N-l_0)e^{-(N-l_0)^2/\bar{l}^2\tau} + \kappa^{-l_0} l_0\, e^{-l_0^2/\bar{l}^2\tau} - \kappa^{-l_0}(N+l_0)\, e^{-(N+l_0)^2/\bar{l}^2\tau}]/l\pi^{1/2}\tau^{3/2}\,. \quad \text{(B9)}$$

The first passage-time distribution $\tilde{F}(N-l_0, \tau)$ consists of a sum of terms of the form $\beta\tau^{-3/2}e^{-\beta^2/t}$. The characteristic function for $\tilde{G}(l, \tau)$ computed with $\psi_2(t)$ has been given previously,[15]

$$\gamma(k, \tau) = \tfrac{1}{2}\lambda^{-1/2}(k)\sum_{\pm}(\pm)\, c_\pm\, e^{\tau c_\mp^2}\operatorname{erfc}(\tau^{1/2}c_\mp)\,, \quad \text{(B10)}$$

$$c_\pm \equiv 1 \pm \lambda^{1/2}(k)\,, \quad \text{(B11)}$$

$$\lambda(k) = 1 - 2p + 2p\tilde{\eta}e^{-ik} + 2p(1-\tilde{\eta})\,e^{ik}\,. \quad \text{(B12)}$$

Thus, inserting Eqs. (B10) and (B9) into Eq. (B4), one must calculate integrals of the form

$$\frac{\beta}{\pi^{1/2}}\int_0^\infty d\tau'\, \frac{e^{-\beta^2/\tau'}}{\tau'^{3/2}}\, e^{c^2(\tau-\tau')}\operatorname{erfc}[c(\tau-\tau')^{1/2}]\,, \quad \text{(B13)}$$

in order to determine $\Gamma(k, \tau)$. We introduce a new integration variable $t = (\tau/\tau') - 1$ and change Eq. (B13) to

$$\frac{\beta e^{-\beta^2/\tau}}{(\pi\tau)^{1/2}}\int_0^\infty \frac{dt\, e^{-(\beta^2/\tau)t}}{(t+1)^{1/2}} \times e^{-c^2\tau t/(t+1)}\operatorname{erfc}\{c\tau^{1/2}[t/(t+1)]^{1/2}\}\,. \quad \text{(B14)}$$

The integral in Eq. (B14) now has the form of a Laplace transform. We take advantage of this by inserting into Eq. (B14) the series expression

$$e^{z^2}\operatorname{erfc} z = \sum_{n=0}^{\infty}\frac{(-z)^n}{\Gamma(\frac{1}{2}n+1)} \quad \text{(B15)}$$

and use formula 2.9 of Ref. 17

$$\int_0^\infty \frac{e^{-pt}t^{\nu-1}dt}{(t+a)^{\nu-1/2}} = 2^{\nu-1/2}\Gamma(\nu)p^{-1/2}\,e^{ap/2}D_{1-2\nu}[(2ap)^{1/2}]\,, \quad \text{(B16)}$$

where D_ν is the parabolic cylinder function. We obtain for Eq. (B14)

$$e^{-\beta^2/\tau}\sum_{n=0}^{\infty}(-2c\tau^{1/2})^n e^{\beta^2/\tau} i^n\operatorname{erfc}(\beta/\tau^{1/2})\,, \quad \text{(B17)}$$

where $i^n\operatorname{erfc}$ is the nth repeated integral of the error function. We now insert the integral representation of $e^{z^2} i^n\operatorname{erfc} z$ into Eq. (B17) and sum the series:

$$\frac{2e^{-\beta^2/\tau}}{\pi^{1/2}}\int_0^\infty ds\sum_{n=0}^{\infty}\frac{(-2c\tau^{1/2}s)^n}{n!}\, e^{-s^2-2s\beta/\tau^{1/2}} = \frac{2e^{-\beta^2/\tau}}{\pi^{1/2}}\int_0^\infty ds\exp[-s^2 - 2(\beta\tau^{-1/2} + c\tau^{1/2})s] = e^{-\beta^2/\tau}\exp[(\beta\tau^{-1/2} + c\tau^{1/2})^2] \times\operatorname{erfc}(\beta\tau^{-1/2} + c\tau^{1/2}) \equiv f(\beta, c; \tau)\,. \quad \text{(B18)}$$

Thus the final expression for the characteristic function is

$$\Gamma(k, \tau) = \gamma(k, \tau)\, e^{-il_0k} - \tfrac{1}{2}\lambda^{-1/2}(k)\sum_{\pm}(\pm)c_\pm \times\left[f\left(\frac{N-l_0}{\bar{l}}, c_\mp; \tau\right) + \kappa^{-l_0}f\left(\frac{l_0}{\bar{l}}, c_\mp; \tau\right) - \kappa^{-l_0}f\left(\frac{N+l_0}{\bar{l}}, c_\mp; \tau\right)\right]\,. \quad \text{(B19)}$$

This expression is used in the numerical inversion of Eq. (B2) to obtain the $\tilde{P}(l, \tau)$ shown in Figs. 12–14.

APPENDIX C: GENERAL ASYMPTOTIC EVALUATION OF THE FIRST PASSAGE-TIME DISTRIBUTION $F(N-l_0\tau)$

As shown by Eqs. (34) and (37), and discussed in Appendix B, the solution for the propagator in the presence of absorbing boundaries involves the evaluation of the first passage-time distribution $\tilde{F}(N-l_0, \tau)$. In the region of interest, $\tau \gg 1$, $\tilde{F}(N-l_0, \tau)$ can be determined from the small-s behavior of its Laplace transform. Following Eqs. (B5-B7), one needs to consider integrals of the form

$$f(\tau) = \frac{1}{2\pi i}\int_{c-i\infty}^{c+i\infty} ds\, e^{s\tau}e^{-bs^\alpha}\,, \quad \text{(C1)}$$

corresponding to

$$1 - \tilde{\psi}(s) \propto s^\alpha\,. \quad \text{(C2)}$$

The function $f(\tau)$ is essentially a Levy distribution.[24] The final expression for $\tilde{F}(N-l_0, \tau)$ contains a sum of terms, each proportional to Eq. (C1) for various values of the constant b. By a simple change in the integration variable, one can group the parameters of the integral in Eq. (C1) to obtain

$$\tau f(\tau) = \frac{1}{2\pi i}\int_{\tilde{c}-i\infty}^{\tilde{c}+i\infty} dz\exp[z - (b/\tau^\alpha)z^\alpha]\,. \quad \text{(C3)}$$

We can now evaluate the integral in Eq. (C3) in two time regimes: (a) $b/\tau^{\alpha} \ll 1$, and (b) $b/\tau^{\alpha} \gg 1$. The constant b is typically a large number ($\sim N/\bar{l}$), so both regimes correspond to $\tau \gg 1$ [therefore justifying the use of Eq. (C1)]. The transition regime $b/\tau^{\alpha} \gtrsim 1$ corresponds to the transit time. In regime (a) one can develop an asymptotic series for $\tau f(\tau)$ by expanding $\exp(-bz^{\alpha}/t^{\alpha})$ and integrating term by term,

$$\tau f(\tau) = \sum_{l=0}^{\infty} \frac{1}{l!} \left(-\frac{b}{\tau^{\alpha}}\right)^{l} \frac{1}{2\pi i} \int_{C} dz\, z^{l\alpha} e^{z} . \tag{C4}$$

The contour C in Eq. (C4) is shown in Fig. 16. The original contour in Eq. (C3) is displaced, to the left in the z plane, to one consisting of a broken circle around the branch point at the origin and line segments parallel to the imaginary axis (dotted line). The latter part of contour makes an exponentially small contribution and thus, the countour can be further changed to C. The integral in Eq. (C4) is simply the Hankel representation of the inverse Γ function,[25] thus

$$\tau f(\tau) = \sum_{l=0}^{\infty} \frac{(-b/\tau^{\alpha})^{l}}{\Gamma(l+1)\Gamma(-l\alpha)} . \tag{C5}$$

Now, $1/\Gamma(-l\alpha) = 0$ for $l\alpha = 0, 1, 2, 3, \ldots$. For such values of $l\alpha$, there is no branch point, and hence the integral evaluated on C vanishes. The above derivation of Eq. (C5) is essentially a proof of the Tauberian theorem.

Now, using the familiar reflection formula for the γ function

$$\Gamma(z)\Gamma(1-z) = \pi \csc \pi z , \tag{C6}$$

one can rewrite Eq. (C5) as

$$\tau f(\tau) = -\frac{1}{\pi} \sum_{l=0}^{\infty} \left(\frac{-b}{\tau^{\alpha}}\right)^{l} \sin \pi l\alpha \, \frac{\Gamma(l\alpha+1)}{\Gamma(l+1)} . \tag{C7}$$

Using the well-known asymptotic properties of the gamma function, one can see that the function defined by the sum in Eq. (C7) is an entire function for $0 < \alpha < 1$. For some values of α, where $\Gamma(l\alpha + 1)$ is a factor of $\Gamma(l+1)$, one can analytically sum the series:

$$\alpha = \tfrac{1}{2} , \quad \tau f(\tau) = \frac{b}{2\pi^{1/2}\tau^{1/2}} e^{-b^2/4\tau} , \tag{C8}$$

$$\alpha = \tfrac{1}{3} , \quad \tau f(\tau) = \frac{\sin(\pi/3)}{\pi} x K_{1/3}(x) ,$$

$$x \equiv 2\left(\frac{b}{3\tau^{1/3}}\right)^{3/2} , \tag{C9}$$

where $K_{\nu}(x)$ is the modified Bessel function of order ν. More generally, for any rational value of α, $\tau f(\tau)$ can be represented as a finite sum of generalized hypergeometric functions ${}_iF_k(a_1, \ldots, a_i; c_1, \ldots, c_k; x)$, e.g.,

$$\alpha = \tfrac{3}{4} , \quad \tau f(\tau) = -\left(\frac{8}{3\pi}\right)^{1/2} \sum_{n=1}^{3} \sin\left(\frac{3\pi n}{4}\right) z^{n} \times {}_2F_2\left(\frac{1}{3} + \frac{n}{4}, \frac{2}{3} + \frac{n}{4}; \frac{1}{2} + \frac{n(n-1)}{8}, \frac{n(7-n)}{8}; -z^{4}\right) , \quad z \equiv -\frac{b}{4}\left(\frac{\tau}{3}\right)^{-3/4} . \tag{C10}$$

In regime (b) one can evaluate the integral in Eq. (C3) with the saddle-point method.[26] One seeks the stationary points of $z - (b/\tau^{\alpha})z^{\alpha}$, i.e.,

$$z_0 = (ab/\tau^{\alpha})^{1/(1-\alpha)} . \tag{C11}$$

Expanding the exponent in (C3) about z_0 one finds that the path of steepest descent through z_0 is parallel to the imaginary axis. Hence,[27]

$$\tau f(\tau) \simeq \frac{\exp\{-[(1-\alpha)/\alpha](\alpha b/\tau^{\alpha})^{1/(1-\alpha)}\}}{[2\pi(1-\alpha)(\tau^{\alpha}/\alpha b)^{1/(1-\alpha)}]^{1/2}} , \quad \frac{b}{\tau^{\alpha}} \gg 1 . \tag{C12}$$

We can now compare the general asymptotic form to the analytic results in Eqs. (C8) and (C9). For $\alpha = \frac{1}{2}$ the expression in Eq. (C12) is exact, and is equal to Eq. (C8). For $\alpha = \frac{1}{3}$, we must first obtain the asymptotic limit of Eq. (C9). For $x \to \infty$,

$$x K_{1/3}(x) \to (\pi x/2)^{1/2} e^{-x}$$

and

$$\tau f(\tau) \simeq (3/4\pi)^{1/2} (b/3\tau^{1/3})^{3/4} \exp[-2(b/3\tau^{1/3})^{3/2}] . \tag{C13}$$

The expression agrees exactly with the one in Eq. (C12) for $\alpha = \frac{1}{3}$. Hence, we have been able to establish a representation of the function $\tau f(\tau)$ in both time regimes of pertinence to our transport study.

The function in Eq. (C1) is, as mentioned above, the Levy distribution, and therefore of interest in other areas of stochastic processes. The representation of $f(\tau)$ we have established will be further developed in another paper.

APPENDIX D: CALCULATION OF $\psi(t)$

We outline the main steps in the computation of $\psi(t)$; the details can be found in Ref. 14. We consider an arbitrary site as the origin in a random medium and define $Q(t)$ to be equal to the probability that a carrier remains on the site for a time interval t after arrival. This probability can decrease in time via all the *parallel decay channels* for it to transfer to surrounding sites:

$$\frac{dQ}{dt} = -Q \sum_{j} W(\vec{r}_j) , \tag{D1}$$

where $W(\vec{r})$ is the transition rate to a site located at $\vec{r}$. One now solves (D1) for the fixed (random) configuration $\{r_j\}$, computes the configuration average,

$$\Psi(t) \equiv \langle Q(t) \rangle = \left\langle \exp\left[-t \sum W(\vec{r}_j) \right] \right\rangle$$
$$= \exp\left(- \int d^3r\, p(\vec{r}) \{ 1 - \exp[- W(\vec{r}) t] \} \right) , \tag{D2}$$

and determines $\psi(t)$ with the relation

$$\psi(t) = - \frac{d\Psi(t)}{dt} . \tag{D3}$$

In Eq. (D2), $p(\vec{r})d^3r$ is the probability a site is located in a volume d^3r centered about $\vec{r}$. An excellent approximation to the integrand in Eq. (D2) in the limit of large τ (cf. Appendix A of Ref. 14) is a unit step function,

$$1 - \exp[- W(\vec{r}) t] = \begin{cases} 1, & W(\vec{r}) t > 1 \\ 0, & W(\vec{r}) t < 1 . \end{cases} \tag{D4}$$

Due to the general exponential dependence of $W(\vec{r})$ on r, the transition from 1 to 0 in Eq. (D4) is very rapid as a function of $\vec{r}$. With

$$W(\vec{r}) = W_M e^{-r/Rd} , \tag{D5}$$

the assumption of a totally random distribution

$$p(\mathbf{r}) = N_D , \tag{D6}$$

and the use of Eq. (D4), one obtains

$$\ln\Psi(t) = -4\pi N_D \int_0^{r_\tau} r^2 dr = -4\pi N_D r_\tau^3/3 , \tag{D7}$$

where

$$W(r_\tau) t \equiv \tau e^{-r_\tau / R_d} = e^{-c} \simeq 1 , \tag{D8}$$

or

$$r_\tau = R_d \ln e^{c\tau} . \tag{D9}$$

We now absorb the constant e^c into the definition of W_M and, inserting Eqs. (D7) and (D9) into (D3), one has

$$\frac{\psi(t)}{W_M} = \frac{-d\Psi}{d\tau} = \frac{\eta(\ln\tau)^2}{\tau^{1+(\eta/3)(\ln\tau)^2}} , \quad \tau \gg 1 , \tag{D10}$$

which is the result we quoted for $\psi_h(t)$ in Eq. (60). The long tail in $\psi(t)$ is related to the absence of a truncation of the transition rate spectrum, i.e., at an arbitrary t one can "find," with a finite probability, a $W(\vec{r})$, such that $W(\vec{r})t \simeq 1$. The "smoothness" of the tail is related to the random assumption (D6). If instead of Eq. (D5) one used

$$W(\vec{r}) = W_M \exp[- (r/R_D)^\gamma] , \tag{D11}$$

with $\gamma \geq 1$, then

$$r_\tau = R_d (\ln \tau)^{1/\gamma} \tag{D12}$$

and

$$\Psi(t) = \exp[- (\eta/3) (\ln \tau)^{3/\gamma}] . \tag{D13}$$

Hence for $\gamma > 1$, the time dependence of $\psi(t)$ would be slower than Eq. (D10) for a given value of η. *The more rapid the dependence of $W(r)$ on r, the slower the time decay of $\psi(t)$!* If one can change $W(r)$ significantly by a small variation in r, then for any arbitrary t one can locate a nearest-neighbor site separation that satisfies $W(r)t \simeq 1$. There is direct experimental verification of these concepts in the study of radiative recombination in semiconductors.[14,28]

---

*Partially supported by ARPA and monitored by ONR (N00014-17-0308).

[1]A. R. Adams and W. E. Spear, J. Phys. Chem. Solids 25, 1113 (1964); D. J. Gibbons and W. E. Spear, J. Phys. Chem. Solids 27, 1917 (1966).
[2]W. E. Spear, Proc. Phys. Soc. Lond. B 70, 669 (1957).
[3]M. D. Tabak and P. J. Warter, Phys. Rev. 173, 899 (1968); D. M. Pai and S. W. Ing, Phys. Rev. 173, 7[illegible] (1968).
[4]P. G. LeComber and W. E. Spear, Phys. Rev. Lett. 25, 509 (1970).
[5]N. F. Mott, J. Non-Cryst. Solids 1, 1 (1968).
[6]A. Many and G. Rakavy, Phys. Rev. 126, 1980 (1962).
[7]D. M. Pai (private communication).
[8]M. E. Sharfe, Phys. Rev. B 2, 5025 (1970); D. M. Pai and M. E. Scharfe, J. Non-Cryst. Solids 8–10, 752 (1972); M. E. Scharfe, Bull. Am. Phys. Soc. 18, 454 (1973); M. E. Scharfe (private communication).
[9]G. Pfister, Phys. Rev. Lett. 33, 1474 (1974); and private communication.
[10]J. Mort and A. I. Lakatos, J. Non-Cryst. Solids 4, 117 (1970). The first mention of the universal shape of $I(t)$ is contained in this reference.
[11]W. D. Gill, J. Appl. Phys. 43, 5033 (1972).
[12]M. Silver, K. S. Dy, and D. L. Huang, J. Non-Cryst. Solids 8–10, 773 (1972).
[13]V. M. Kenkre, E. W. Montroll, and M. F. Shlesinger, J. Stat. Phys. 9, 45 (1973).
[14]H. Scher and M. Lax, Phys. Rev. B 7, 4491 (1973); 7, 4502 (1973).
[15]E. W. Montroll and H. Scher, J. Stat. Phys. 9, 101 (1973).
[16]M. Shlesinger, J. Stat. Phys. 10, 421 (1974).
[17]G. E. Roberts and H. Kaufman, *Tables of Laplace Transforms* (Saunders, Philadelphia, 1966).
[18]A preliminary account of this analysis has appeared in H. Scher, *Amorphous and Liquid Semiconductors*, edited by J. Stuke and W. Brenig (Taylor and Francis, London, 1974), p. 135.
[19]S. C. Maitra and H. Scher (unpublished).
[20]M. L. Knotek, M. Pollak, and T. M. Donovan, in Ref. 18, p. 225.
[21]H. Seki, in Ref. 18, p. 1015.
[22]G. Weiser, J. Appl. Phys. 43, 5028 (1972).
[23]W. Feller, *An Introduction to Probability Theory and its Applications*, 2nd ed. (Wiley, New York, 1971), Vol II.
[24]P. Levy, *Processus Stochastiques et Mouvement Brownien*, 2nd ed. (Gauthier-Villars, Paris, 1965).
[25]Formula No. 6.1.4 in *Handbook of Mathematical Func-*

tions, edited by M. Abramowitz and I. A. Stegun (U. S. GPO, Washington, D. C. 1964).

[26]E. T. Copson, *Asymptotic Expansions* (Cambridge U.P., Cambridge, England, 1965).

[27]We have discovered that similar functions have been discussed in E. W. Barnes, Phil. Trans. Roy. Soc. A 206, 249 (1906).

[28]D. G. Thomas, J. J. Hopfield, and W. M. Augustyniak, Phys. Rev. 140, A202 (1965); R. C. Enck and A. Honig, Phys. Rev. 177, 1182 (1969).